Supplementary Information

Visible Light-Induced Olefin Activation using 3D Aromatic Boron-Rich Cluster Photooxidants

Marco S. Messina,[a],[b] Jonathan C. Axtell,[a] Yiqun Wang,[a],[b], Paul Chong,[a] Alex I. Wixtrom,[a] Kent O. Kirlikovali,[a] Brianna M. Upton,[a],[b],[c] Bryan M. Hunter,[d] Oliver S. Shafaat,[d] Saeed I. Khan,[a] Jay R. Winkler,[d] Harry B. Gray,[d] Anastassia N. Alexandrova,[a],[b] Heather D. Maynard,[a],[b] and Alexander M. Spokoyny*[a]

[a]Department of Chemistry and Biochemistry, University of California, Los Angeles, 607 Charles E. Young Drive East, Los Angeles, California 90095-1569, United States.

[b]California NanoSystems Institute, University of California, Los Angeles, 570 Westwood Plaza, Los Angeles, California 90095-1569, United States.

[c]Department of Bioengineering, University of California, Los Angeles, 410 Westwood Plaza, Los Angeles, California 90095-1600, United States

[d] Beckman Institute, California Institute of Technology, Pasadena, California, 91115, United States

*Correspondence to: spokoyny@chem.ucla.edu

Table of Contents

I. General Information

Methods and Materials

Reagent Information:

All commercially available chemicals were used as received unless otherwise stated. All polymerizations were prepared in the glovebox under nitrogen atmosphere unless otherwise stated. All solvents were purified via a solvent purification system and kept in the glovebox. All monomers were degassed and stored with 4Å molecular sieves. 4-Vinylanisole (97%), 4-methylstyrene (96%), styrene (≥99%), 4-fluorostyrene (99%), 4-*tert*-butylstyrene (93%), 4-chlorostyrene (97%), 3-chlorostyrene (98%), and 2,6-difluorostyrene (99%) were purchased from Sigma-Aldrich. *Closo*-dodecahydrododecaborate ($[NEt_3H]_2[B_{12}H_{12}]$) was purchased from Boron Specialties (USA). Ethanol (200 proof) was purchased from Decon Labs and used as received. Iron(III) chloride hexahydrate (≥97%), cesium hydroxide monohydrate (≥99.5%), hydrogen peroxide (30% in H_2O), tetrabutylammonium hydroxide (40% in H_2O), acetonitrile (≥99.9%), dichloromethane (≥99.5%), ethyl acetate (≥99.5%), hexanes (≥98.5%), methanol (≥99.8%), N,N-diisopropylethylamine (≥99%), and tetrabutylammonium hexafluorophosphate (≥99.0%, electrochemical grade), 2-methylpropene (99%) were purchased from Sigma-Aldrich. Tetrabutylammonium hexafluorophosphate was further purified by recrystallization from ethanol and drying under vacuum at 90 °C and benzyl bromide (99%) was purchased from Alfa Aesar. Tetramethylammonium tetrafluoroborate (>98%) was purchased from TCI.

General Analytical Information:

NMR spectra were recorded using spectrometers at 400 or 500 MHz (^{1}H), 125 MHz (^{13}C), 80 MHz (^{11}B), and 282 MHz (^{19}F) reported in δ (parts per million) relative to tetramethylsilane (^{1}H, ^{13}C), $BF_3{\cdot}Et_2O$ (^{11}B) or C_6H_5F (^{19}F), respectively, and referenced to residual ^{1}H/^{13}C signals of the deuterated solvent (^{1}H (δ) $CDCl_3$ 7.26; ^{13}C (δ) $CDCl_3$ 77.16; ^{11}B (δ) $BF_3{\cdot}Et_2O$ 0.00 ppm; ^{19}F (δ) C_6H_5F -113.15 ppm). Deuterated solvents (Cambridge Isotope Laboratories) for NMR spectroscopic analyses were stored over 4Å molecular sieves. ^{1}H NMR spectra were acquired with a relaxation of 2 s for small molecules and 30 s for polymers. Gel permeation chromatography (GPC) for all polymers was conducted on a Jasco system equipped with a refractive index detector, a UV detector, one Waters Styragel guard column, and four Waters HR Styragel 5 μm columns (100-5K, 500-30K, 50-100K, 5-600 K) using tetrahydrofuran (THF) at 30 °C and a flow rate of 1.0 mL/min. Calibration was performed using near-monodisperse polystyrene standards from Jordi Laboratories and chromatograms were analyzed using ChromNAV chromatography software. GPC for poly-4-methoxystyrene was conducted on a Shimadzu high performance liquid chromatography (HPLC) system with a refractive index RID-10A, one Polymer Laboratories PLgel guard column, and two Polymer Laboratories PLgel 5 μm mixed D columns. Eluent was DMF with LiBr (0.1 M) at 40 °C (flow rate: 0.60 mL/min). Chromatograms from DMF GPC were analyzed using LabSolutions software. GPC was also conducted on a Shimadzu HPLC Prominence-i system equipped with a UV detector, Wyatt DAWN Heleos-II Light Scattering detector, Wyatt Optilab T-rEX RI detector, one MZ-Gel SDplus guard column, and two MZ-Gel SDplus 100 Å 5μm 300x8.0 mm columns. Eluent was $CHCl_3$ at 40 °C (flow rate: 0.70 mL/min). Chromatograms from $CHCl_3$ GPC were analyzed using Astra 6.0 software. Calibration was performed using near-monodisperse polystyrene

standards from Polymer Laboratories. All GPC samples were dissolved in HPLC grade solvent at a concentration of 1-2 mg/mL and filtered through a 0.2 μm TFE filter. All reported molecular weight and dispersity data determined by GPC are the average of two runs unless otherwise noted. A Bruker EMX EPR spectrometer was used to acquire EPR spectra, with all spectra collected in CH_2Cl_2 at ambient temperature. Mass spectrometry data was acquired using a Thermo ScientificTM Q-ExactiveTM Plus instrument with a quadrupole mass filter and Orbitrap mass analyzer. ICP-MS was performed on an Agilent 7500c quadrupole with hydrogen/helium octopole collision cell. Thermogravimetric analysis was performed on a Perkin Elmer Diamon TG/DTA instrument. UV-Vis spectra were recorded on a Hewlett-Packard 8453 diode array spectrometer. Extinction coefficients were determined through a series of 5 dilutions with a maximum absorption between 0.1 and 0.7.

Microwave Reactor Information:

Microwave reactions were performed using a CEM Discover SP microwave synthesis reactor. Except where noted otherwise, all reactions were performed in glass 10 mL microwave reactor vials purchased from CEM with silicone/PTFE caps. Flea micro PTFE-coated stir bars were used in the vials with magnetic stirring set to high and 15 seconds of premixing prior to the temperature ramping. All microwave reactions were carried out at 140 °C with the pressure release limit set to 250 psi (no reactions exceeded this limit to trigger venting) and the maximum wattage set to 250W (the power applied was dynamically controlled by the microwave instrument and did not exceed this limit for any reactions). Column chromatography was performed using 2.0 - 2.25 cm inner diameter glass fritted chromatography columns with 20-30 cm of slurry-packed silica gel to ensure full separation of reagents and products. Unfiltered pressurized air was used to assist column chromatography.

LED Light Source:

Irradiation of photochemical polymerizations were performed utilizing a 120V Blue LED Custom Rope Light Kit ½" 2 wire 3 foot cable purchased from Novelty Lights, Inc. (Eaglewood, CO).

Cyclic Voltammetry Information:

Cyclic voltammetry was performed on using a BAS Epsilon potentiostat with a glassy carbon disc working electrode, platinum wire counter electrode, and Ag/Ag^+ wire pseudoreference. All experiments were conducted in 0.1 M $[NBu_4]PF_6/CH_2Cl_2$ with ~5 mM analyte concentrations. The CH_2Cl_2 was dried in house with a custom drying system running through two alumina columns prior to use. The solution was degassed by bubbling argon, and the cyclic voltammetry was performed under argon gas. A scan rate of 0.1 mV/s was used with Fc/Fc^+ as an external standard.

X-ray data collection and processing parameters

A single crystal of **1b** was mounted on a nylon loop using perfluoropolyether oil and cooled rapidly to 100 K with a stream of cold dinitrogen. Diffraction data were measured using a Bruker APEX-II CCD diffractometer using Mo-K_α radiation. The cell refinement and data reduction were carried out using Bruker SAINT and the structure was solved with SHELXS-97. All subsequent crystallographic calculations were performed using SHELXL-2013

II. Synthetic Procedures for cluster photoinitiators and polymers

Synthesis of $Cs_2B_{12}H_{12}$, $Cs_2B_{12}(OH)_{12}$, and $(NBu_4)_2B_{12}(OH)_{12}$

$CsOH{\cdot}H_2O$ (14.0g, 83.4 mmol) was dissolved in 130 mL methanol in a 300 mL round bottom flask. 13.4 g of triethylammonium dodecahydrododecaborate was added, the reaction was left to stir for 12-18 hours at ambient temperature (~20 ^{0}C). The solution mixture was then filtered through a 60 ml fritted glass funnel and washed with 20 mL methanol three times. The resulting white solid was dried under high vacuum at 50 ^{0}C for 12 hours and characterized by NMR to confirm complete conversion to Cs_2[*closo*-$B_{12}H_{12}$]. Cs_2[*closo*-$B_{12}H_{12}$] was per-hydroxylated to form Cs_2[*closo*-$B_{12}(OH)_{12}$] via previously described methods.[1] The resulting Cs_2[*closo*-$B_{12}(OH)_{12}$] was converted to $(TBA)_2$[*closo*-$B_{12}(OH)_{12}$] (**1**) via previously described methods.[1]

Synthesis of Dodeca(benzyloxy)-*hypercloso*-dodecaborane ($B_{12}(OCH_2Ph)_{12}$, 1a)

$(TBA)_2B_{12}(OH)_{12}$ (50.0 mg, 0.061 mmol) was transferred out of a nitrogen filled glovebox, opened to the air, and dissolved in 1 mL acetonitrile in a 10 mL glass microwave vial. *N,N*-diisopropylethylamine (0.2 mL, 1.15 mmol) and benzyl bromide (1.74 mL, 14.7 mmol) were added along with a magnetic stir bar, the vial was sealed with a Teflon/silicone cap, and the reaction mixture was heated under microwave conditions at 140 ^{0}C with high stirring for 15 minutes. The volatiles were removed via rotary evaporation, and the excess reagent was eluted through a silica column with 65/35 hexanes/ethyl acetate, and the pink/purple product mixture was eluted with dichloromethane. The dichloromethane was removed *via* rotary evaporation, the remaining charged $^{-1/-2}$ product mixture was dissolved in ~5 ml 90/5/5 ethanol/acetonitrile/H_2O, $FeCl_3{\cdot}6H_2O$ (0.3 g, 1.11 mmol) was added and the mixture was left to stir for 12-24 hours. Following oxidation, the solvent mixture was removed via rotary evaporation, and an orange band containing the neutral product was separated from the $FeCl_3{\cdot}6H_2O$ through a silica column with dichloromethane. The dichloromethane was removed *via* rotary evaporation and the final neutral product **1a** was dried under high vacuum to obtain an isolated yield of 63%. Compound **1a** is an orange solid. ^{1}H NMR (500 MHz, $CDCl_3$): δ 7.08 - 7.19 (m, 60H, C_6H_5), 5.25 (s, 24H, O-CH_2). $^{13}C\{^1H\}$ NMR (125 MHz, $CDCl_3$): δ 140.8, 128.4, 127.3, 73.4. $^{11}B\{^1H\}$ NMR (128 MHz, $CDCl_3$): δ 41.8. HRMS (Orbitrap): m/z calculated for $C_{84}H_{84}B_{12}O_{12}$ (M-), 1414.72 Da; found, 1414.72 Da.

Synthesis of Dodeca(pentafluorobenzyloxy)-*hypercloso*-dodecaborane ($B_{12}(OCH_2C_6F_5)_{12}$, 1b)

$(TBA)_2B_{12}(OH)_{12}$ (300 mg, 0.366 mmol) was transferred out of a nitrogen filled glovebox, opened to the air, and dissolved in 4 mL acetonitrile in a 30 mL glass microwave vial. *N,N*-diisopropylethylamine (1.21 mL, 6.96 mmol) and 2,3,4,5,6-pentafluorobenzyl bromide (6.86 mL 45.4 mmol) were added along with a magnetic stir bar, the vial was sealed with a Teflon/silicone cap, and the reaction mixture was heated under microwave conditions at 140˚C with high stirring for 15 minutes. The volatiles were removed via rotary evaporation, and the excess reagent was eluted through a silica column with 65/35 hexanes/ethyl acetate, and the pink/purple product mixture was eluted with acetone. The acetone was removed via rotary evaporation and the residue was dissolved in ~5 mL 90/5/5 ethanol/acetonitrile/H_2O. $FeCl_3{\cdot}6H_2O$ (1.88 g, 6.96 mmol) was added and the mixture was left to stir for 24 hours. The mixture was concentrated *in vacuo*. The residue (while still in the roundbottom flask) was rinsed three times with water. The

residue was then taken up in toluene and extracted three times with water. The organic fractions were combined and dried under vacuum. The resulting solid was charged with hexane and isolated by filtration to afford an orange/yellow solid (574 mg, 63%). ^{1}H NMR (500 MHz, $CDCl_3$): δ 5.23 (s, 24H). ^{13}C NMR (125 MHz, $CDCl_3$): δ 60.1. ^{11}B NMR (160 MHz, $CDCl_3$): δ 40.9. HRMS (Orbitrap): *m/z* calculated for $C_{84}H_{84}B_{12}O_{12}$ (M^-), 2494.1499 Da; found, 2494.1631 Da.

General Procedure for Polymer Synthesis

Styrene (0.05 mL, 0.435 mmol) was passed through activated basic alumina and added to a dram vial equipped with a magnetic stir bar. $B_{12}(OCH_2C_6F_5)_{12}$ (**1b**) (1.1 mg, 0.1 mol%) was then added. This mixture was dissolved in 219 µL dichloromethane, affording a 2M solution of monomer. The dram vial was sealed with a polypropylene cap containing a Teflon coated septum and brought out of the glove box. The mixture was then irradiated with blue LED light (450 nm) (see picture of representative setup below) while stirring for 4 hours at room temperature. For all reactions, the reaction setup is covered with aluminum foil to keep out ambient light. Once the polymerization was complete, the reaction was diluted with ~500 µL dichloromethane and precipitated with cold methanol. The resulting suspension was transferred to a tared falcon tube and centrifuged for 5 minutes at 4,400 RPM. The supernatant was discarded, methanol was then added, stirred to solubilize any excess initiator, and centrifuged again. The supernatant was discarded and the polymer was dried under vacuum. **Polymer conversion experiments:** Polymerizations were set up using optimized conditions (*vide supra*) along with the addition of an equimolar amount of hexamethyldisilane (as an internal reference) with respect to monomer. Aliquots (50 µL) of reaction mixture were taken at given time points and added into a mixture of trimethylamine (5 µL) and $CDCl_3$ (700 µL). Conversions were calculated by ^{1}H NMR spectroscopy by integration of unreacted monomer to hexamethyldisilane.

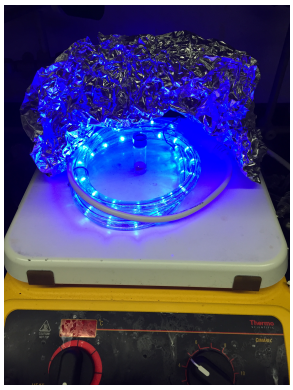

General Procedure for Polymerization of Isobutylene (1-4 psi of Isobutylene)

In the glovebox, **1b** (3.4mg, 1.36 µmol) was added to a Schlenk vessel, equipped with a teflon stopper, containing a magnetic stir bar. Dichloromethane (680 µL) was then added to provide a 2mM solution of **1b**. The vessel was sealed and brought out of the glovebox. The Schlenk vessel containing the mixture was connected to a vacuum transfer bridge; the other outlets were connected to a Schlenk manifold (for vacuum) and the isobutylene regulator (Airgas Part # Y11N570L510), which is connected directly to the isobutylene canister. The entire bridge was

then put under vacuum. The mixture of **1b** was submerged in a dry ice bath until the solvent froze, opened to vacuum for ~5 minutes, and then closed to vacuum and allowed to thaw. This cycle was repeated two more times. The bridge was then closed off from vacuum. Once the mixture containing **1b** thawed, the headspace of the closed system was then backfilled with isobutylene, with the regulator dial set to the desired pressure; for higher amounts of resulting product, 4 psi was used. The mixture of **1b** in CH_2Cl_2 in the isobutylene atmosphere was then irradiated with blue LED light for 4 hours at room temperature with stirring. After 4 hours, the isobutylene source was closed off, and the reaction vessel was carefully vented to let excess isobutylene escape. The mixture was then charged with ~4mL methanol and subsequently all volatiles were removed *in vacuo*. The resulting white residue was qualitatively characterized as highly branched isobutylene by ^{1}H and ^{13}C NMR spectroscopy, with reference to NMR spectra collected by Michl and co-workers (see Volkis, V.; Shoemaker, R. K.; Michl, J. *Macromolecules* **2012**, *45*, 9250-9257).

Electrochemical Bulk Electrolysis (Fe-free) Oxidation of 1b

Microwave synthesis of **1b** was carried out according to the general procedure, excluding the oxidation with $FeCl_3 \cdot 6H_2O$. $[N^nBu_4]_2B_{12}(OH)_{12}$ (99.0 mg, 0.121 mmol) was added to a 10 mL glass microwave vial and transferred out of a nitrogen filled glovebox, opened to air, and dissolved in 2 mL acetonitrile. *N,N*-diisopropylethylamine (0.4 mL, 2.30 mmol) and 2,3,4,5,6-pentafluorobenzyl bromide (1.70 mL, 11.3 mmol) were added along with a flea micro stir bar, the vial was sealed with a PTFE/silicone cap, and the mixture was heated at 140 °C with stirring under microwave conditions for 15 min. The volatiles were removed via rotary evaporation and the excess reagent was eluted through a slurry-packed silica gel column with 65/35 hexanes/ethyl acetate, and the pink/purple product mixture was eluted with CH_2Cl_2. The CH_2Cl_2 was removed via rotary evaporation, and the remaining 2-/1- product mixture was dissolved in 25 mL dichloromethane containing 50 mM tetramethylammonium tetrafluoroborate in a 50 mL beaker. Pt mesh was used as the working electrode, Pt wire inside of a 1 cm diameter glass fritted chamber as the counter electrode, and Ag wire as a pseudoreference electrode. A flea micro stir bar was added, and a potential of -1.3 V was applied for 1 h with stirring. The initially pink solution turned clear outside of the fritted inner chamber, and the solution in the chamber turned orange-red, progressing toward a final yellow-orange color. The fritted chamber containing the yellow-orange solution was removed, the dichloromethane was removed via rotary evaporation, and the remaining yellow-orange solid was dried under high vacuum to yield pure **1b** (5.0 mg, 1.6%). NMR analysis of the product confirmed the complete oxidation of the fraction collected. *Note: This is a non-optimized experiment. The purpose of this procedure was to obtain a small amount of oxidized **1b** without contacting Fe for control experiment use.*

Synthesis of 2,4,6-tri(*p*-tolyl)pyrylium tetrafluoroborate.

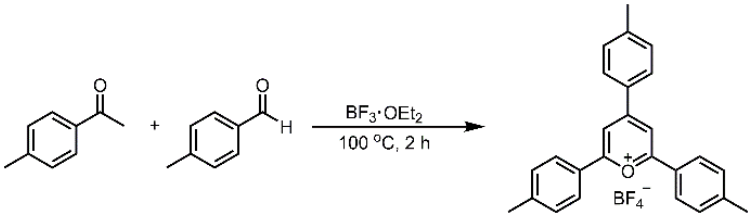

p-Methylacetophenone (5 mL, 5.095 g, 42.4 mmol) and *p*-tolualdehyde (11.32 mL, 11.38 g, 84.8 mmol) were allowed to stir. To this mixture boron trifluoride diethyl etherate (12.56 mL, 14.44 g, 101.8 mmol) was added dropwise. Reaction temperature was then raised to 100 °C and kept stirring for 2 hours. After two hours, reaction was cooled to room temperature and diethyl ether was removed under reduced pressure producing a black oil. To this oil, acetone was added and product was precipitated upon addition of diethyl ether. Product was then collected via filtration and recrystallized five times out of acetone.

III. Cluster Characterization

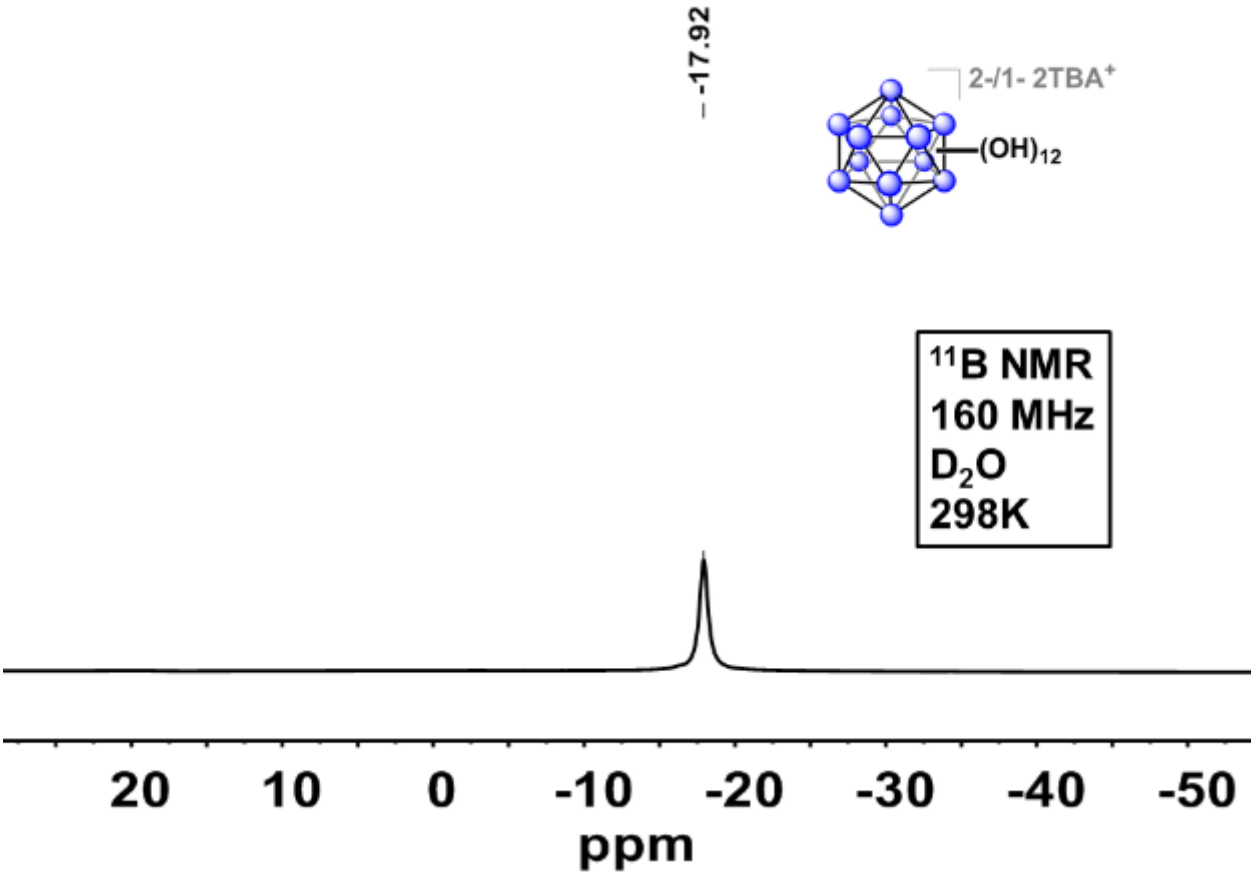

Figure S1: ^{11}B NMR spectrum of *closo*-$B_{12}(OH_{12})$ in D_2O at 298 K.

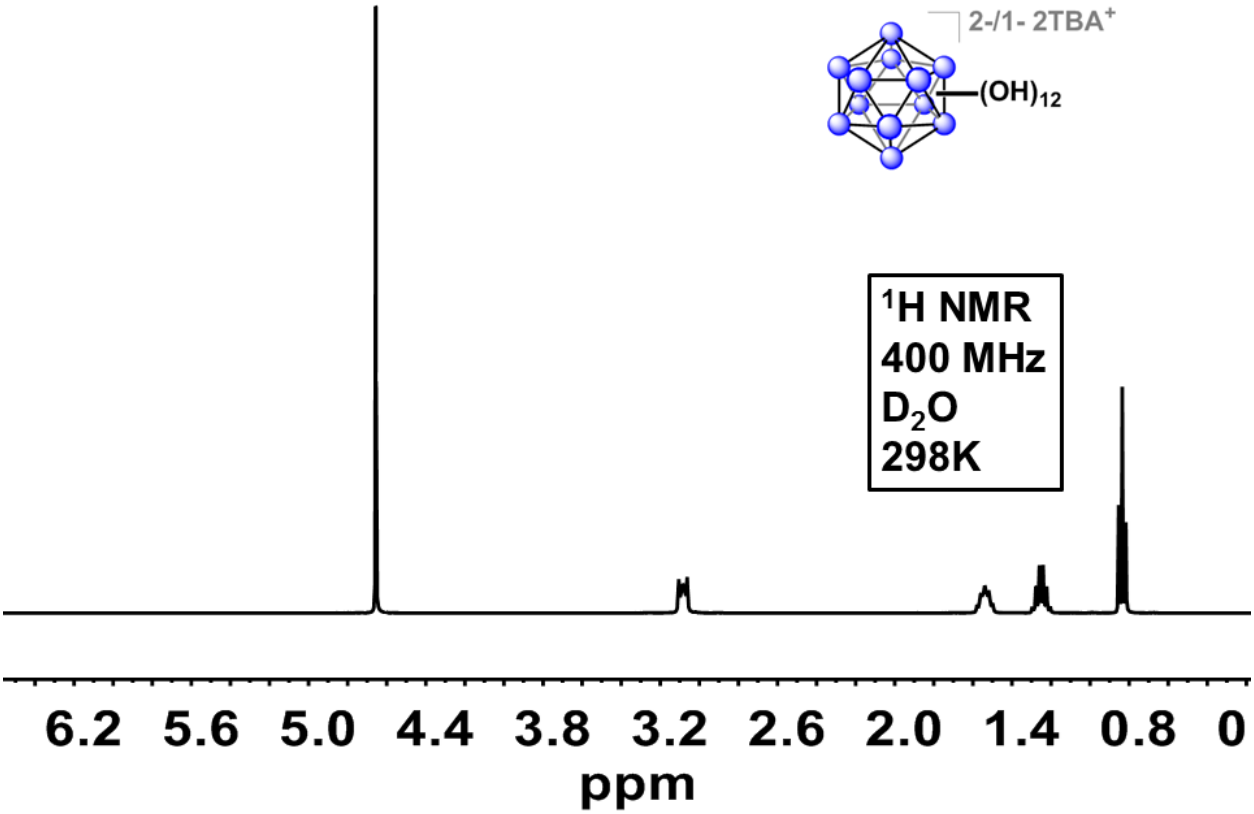

Figure S2: ^{1}H NMR spectrum of *closo*-$B_{12}(OH_{12})$ in D_2O at 298 K.

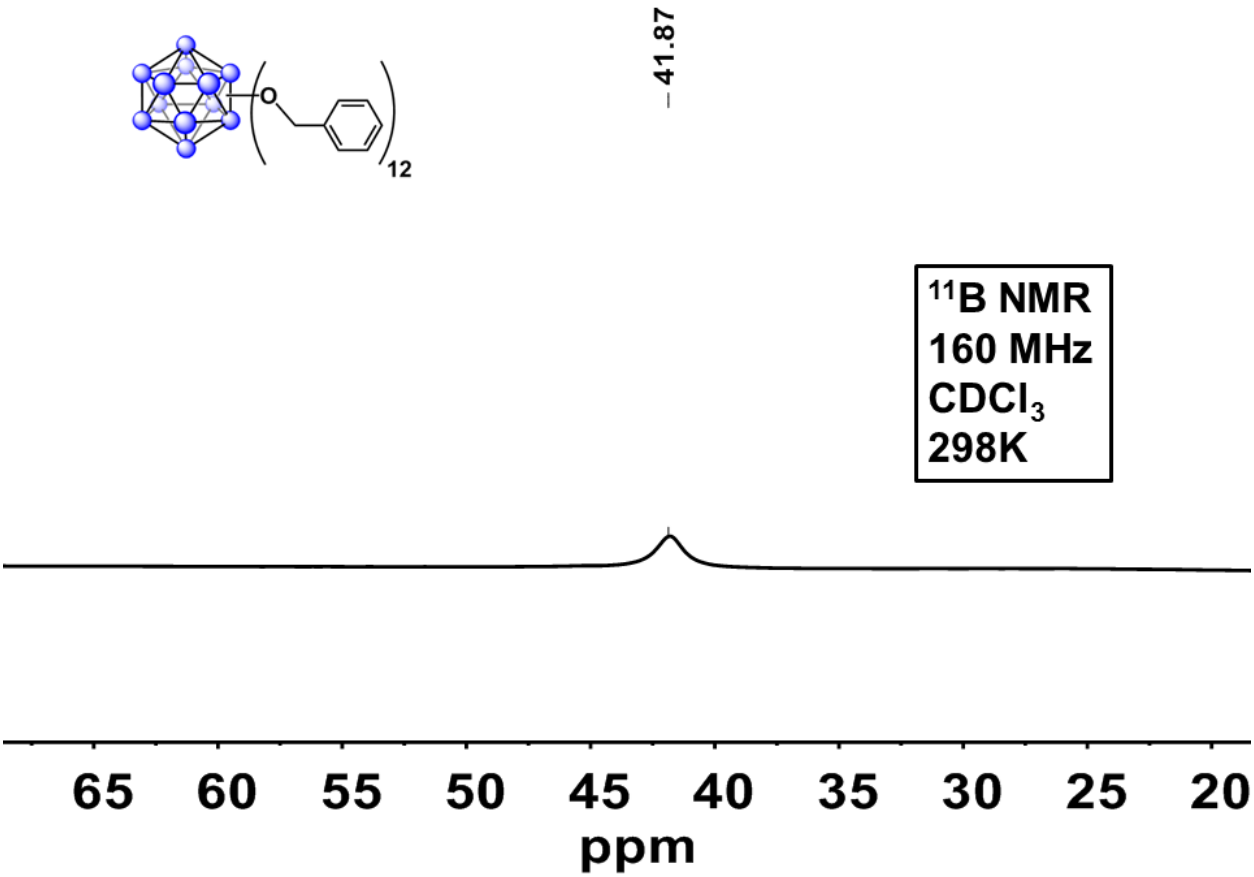

Figure S3: ^{11}B NMR spectrum of $B_{12}(OCH_2Ph)_{12}$ (**1a**) in $CDCl_3$ at 298 K.

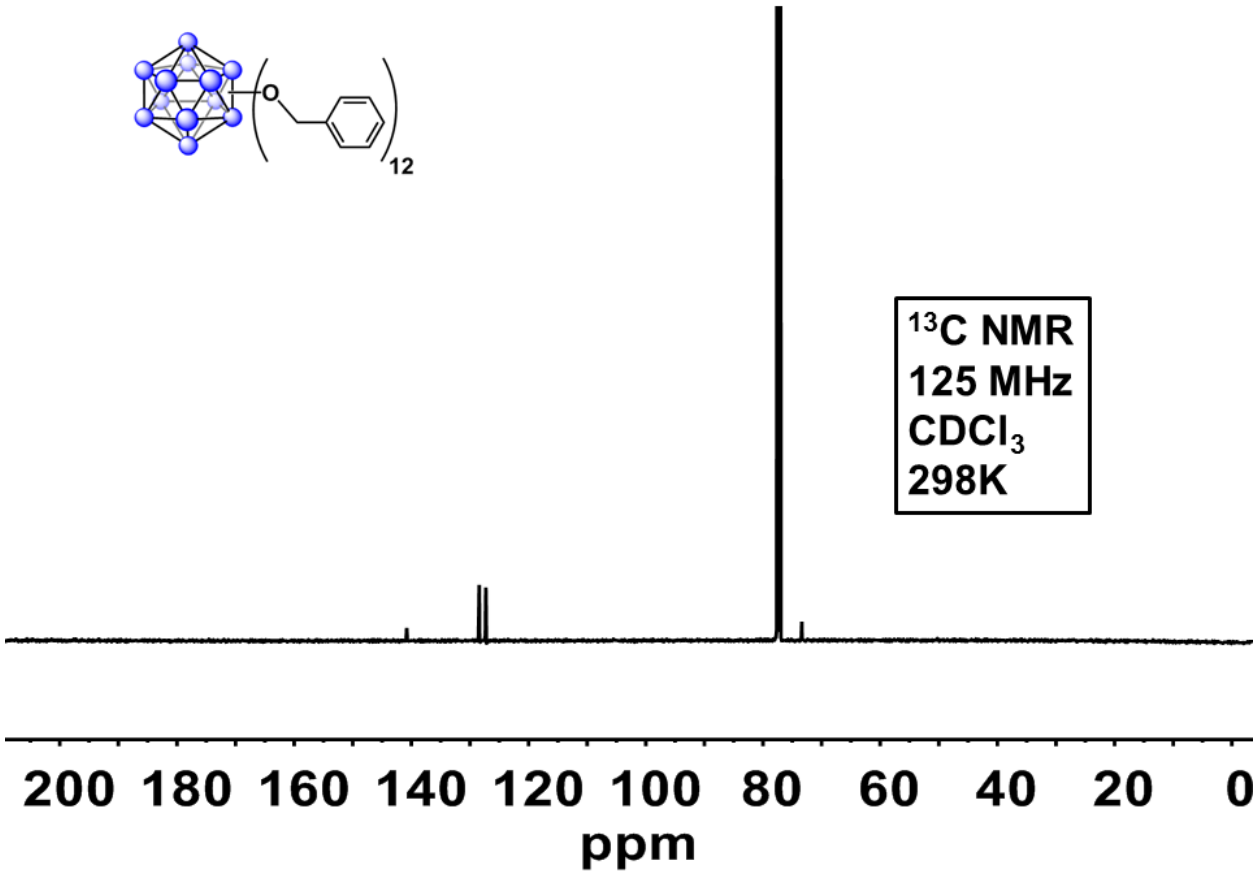

Figure S4: ^{13}C NMR spectrum of $B_{12}(OCH_2Ph)_{12}$ (**1a**) in $CDCl_3$ at 298 K.

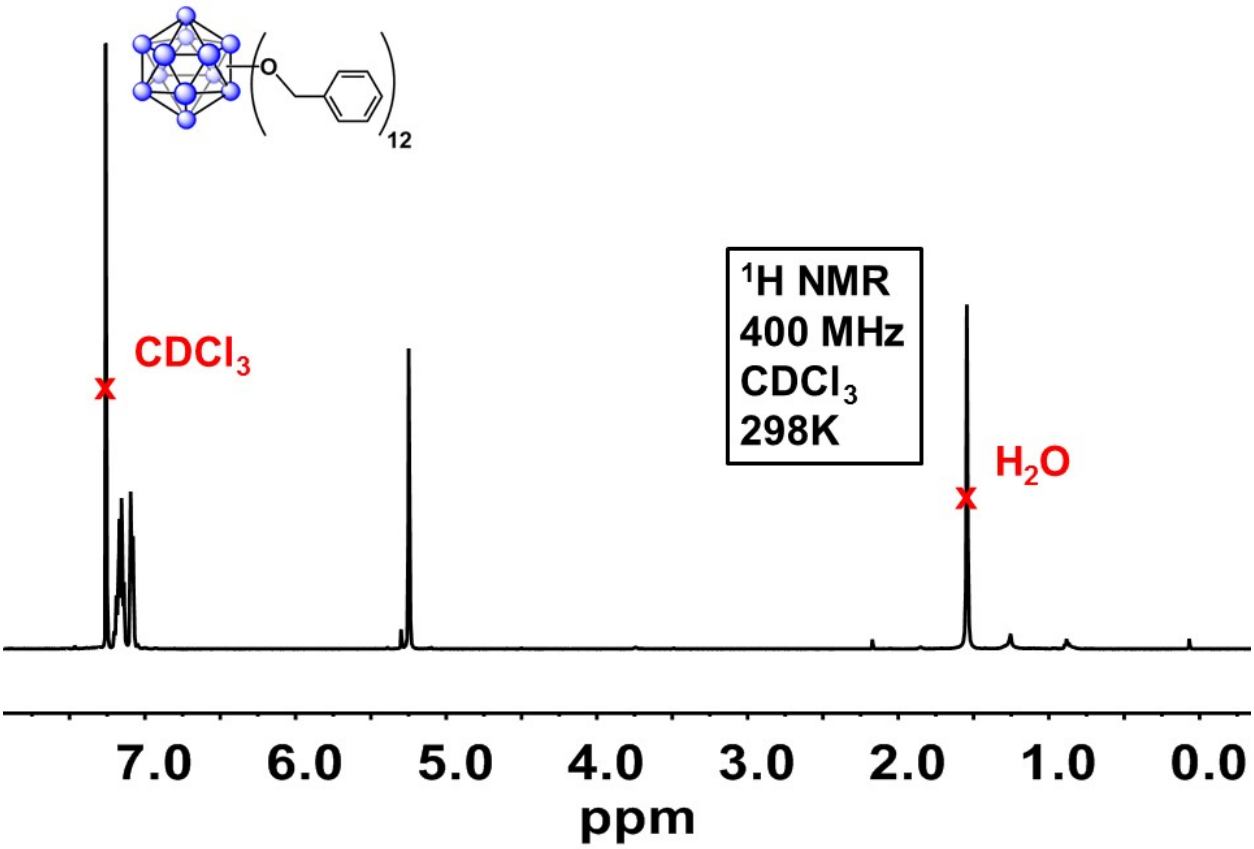

Figure S5: ^{1}H NMR spectrum of $B_{12}(OCH_2Ph)_{12}$ (**1a**) in $CDCl_3$ at 298 K.

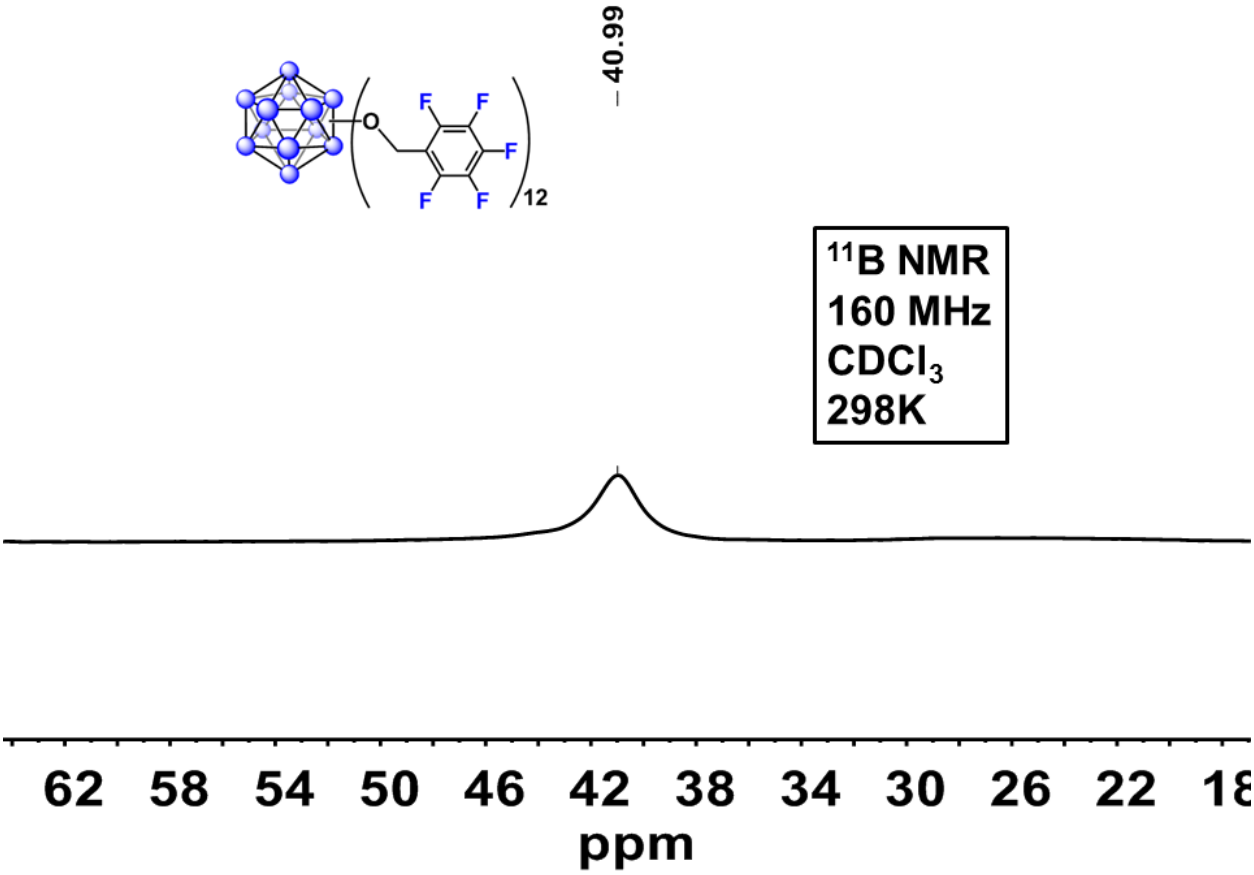

Figure S6: ^{11}B NMR spectrum of $B_{12}(OCH_2C_6F_5)_{12}$ (**1b**) in $CDCl_3$ at 298 K.

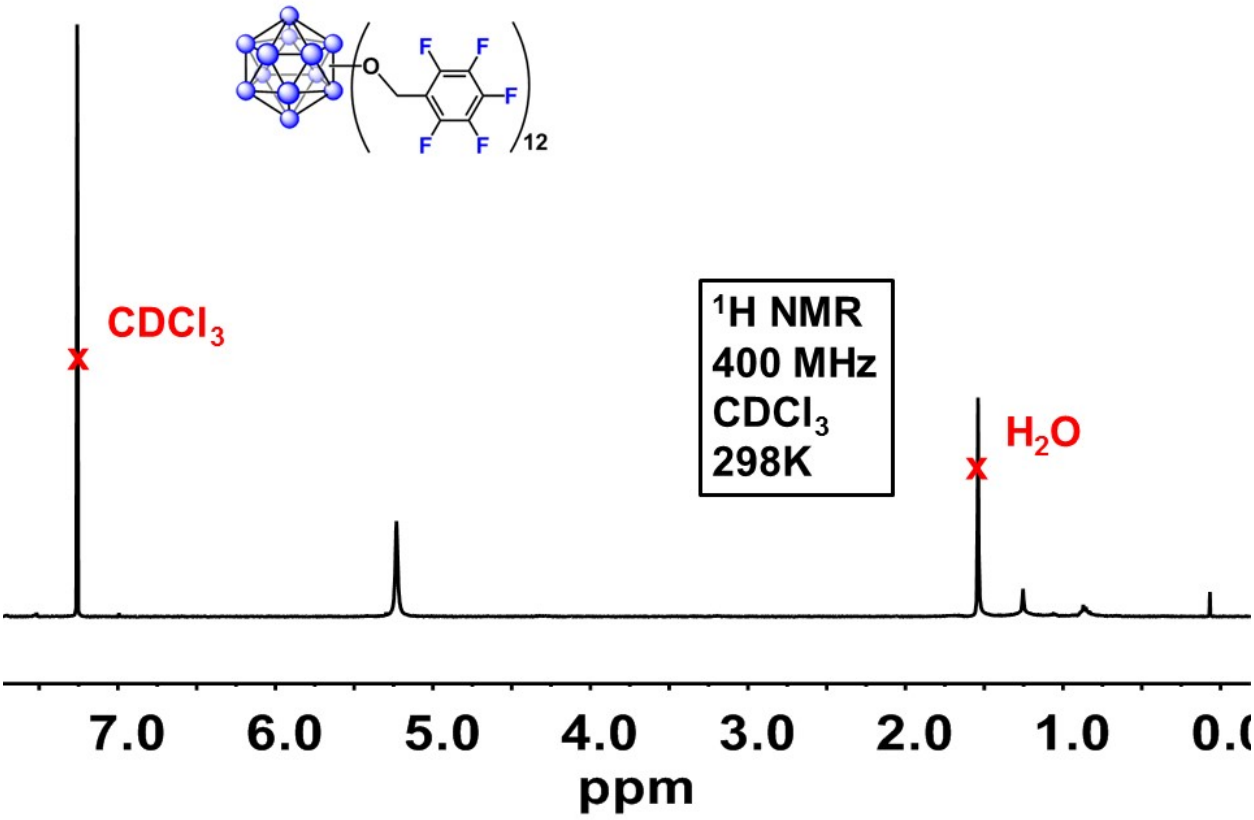

Figure S7: ^{1}H NMR spectrum of $B_{12}(OCH_2C_6F_5)_{12}$ (**1b**) in $CDCl_3$ at 298 K.

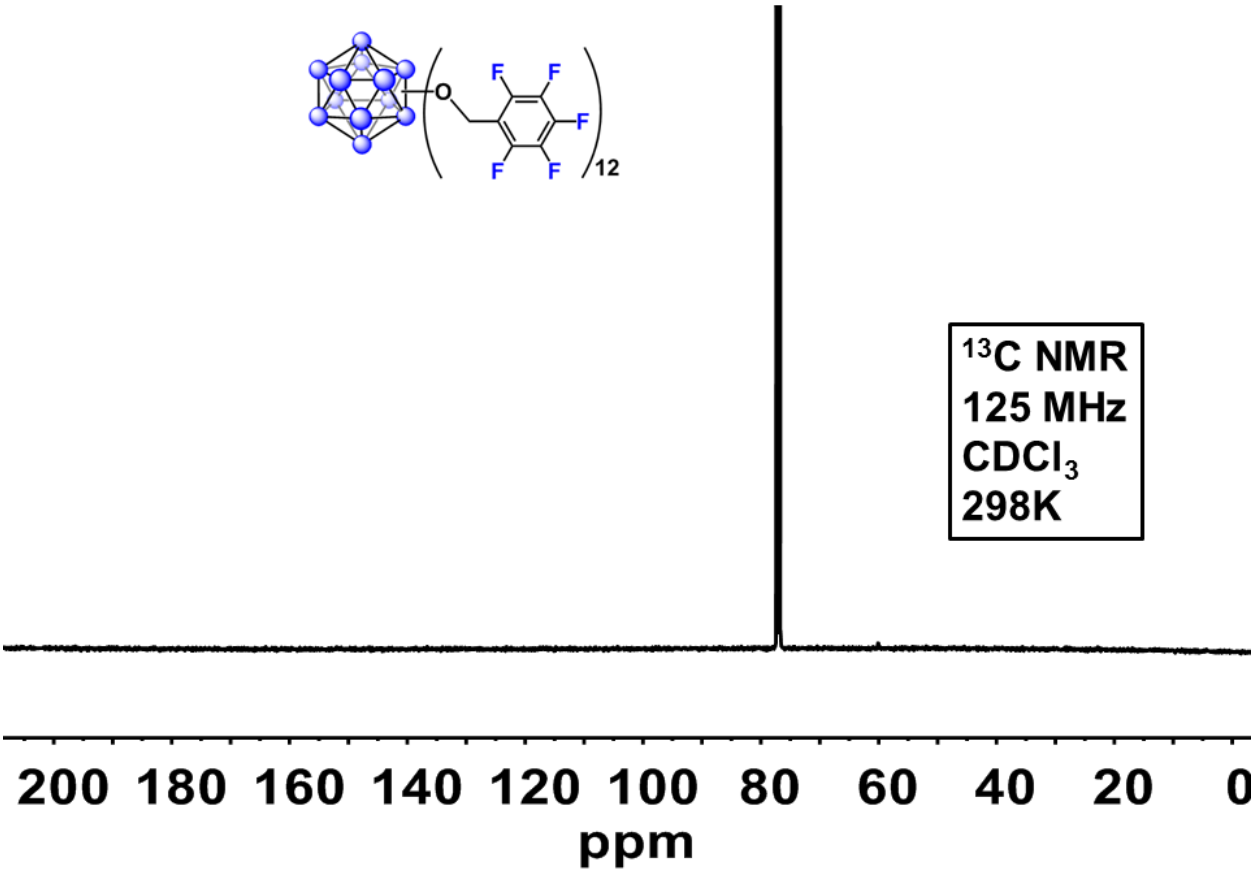

Figure S8: ^{13}C NMR spectrum of $B_{12}(OCH_2C_6F_5)_{12}$ (**1b**) in $CDCl_3$ at 298 K.

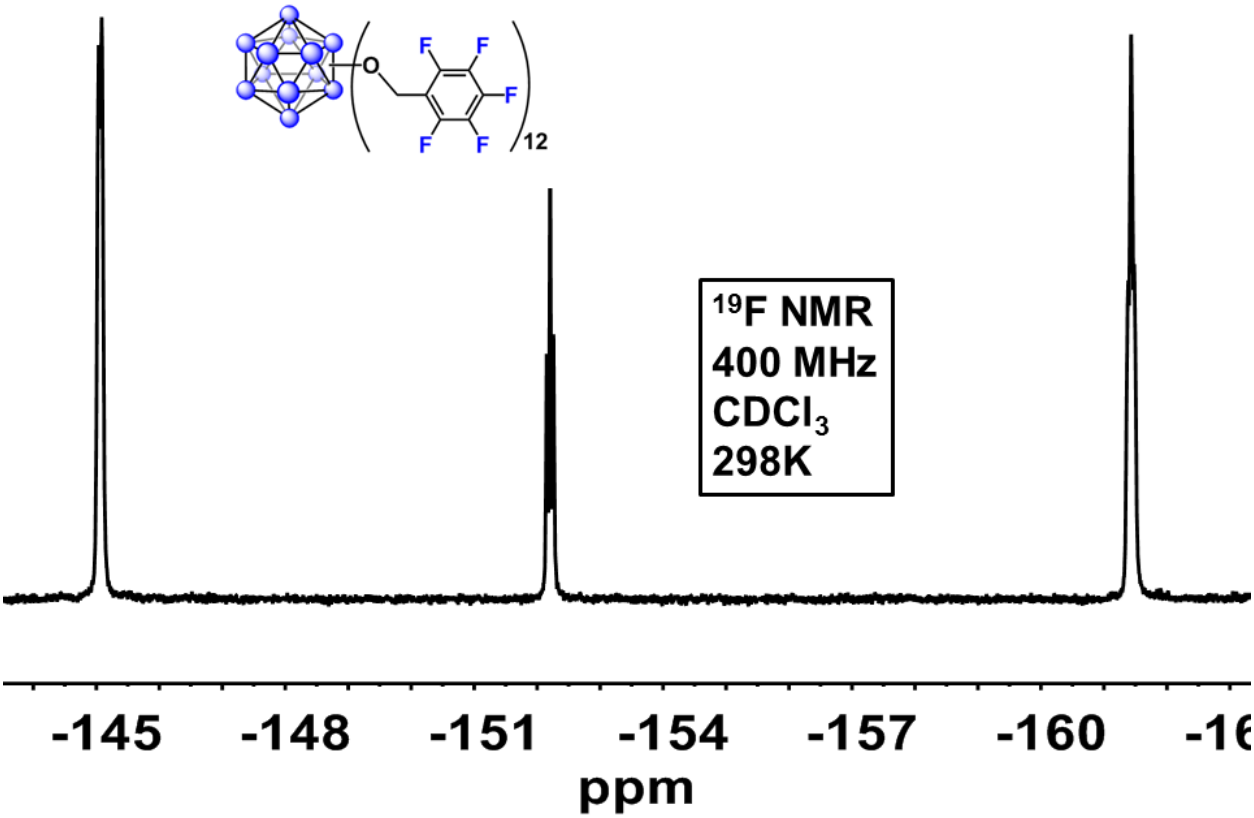

Figure S9: ^{19}F NMR spectrum of $B_{12}(OCH_2C_6F_5)_{12}$ (**1b**) in $CDCl_3$ at 298 K.

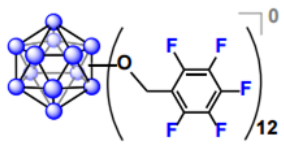

Q Exactive
High-Res Mass Spec

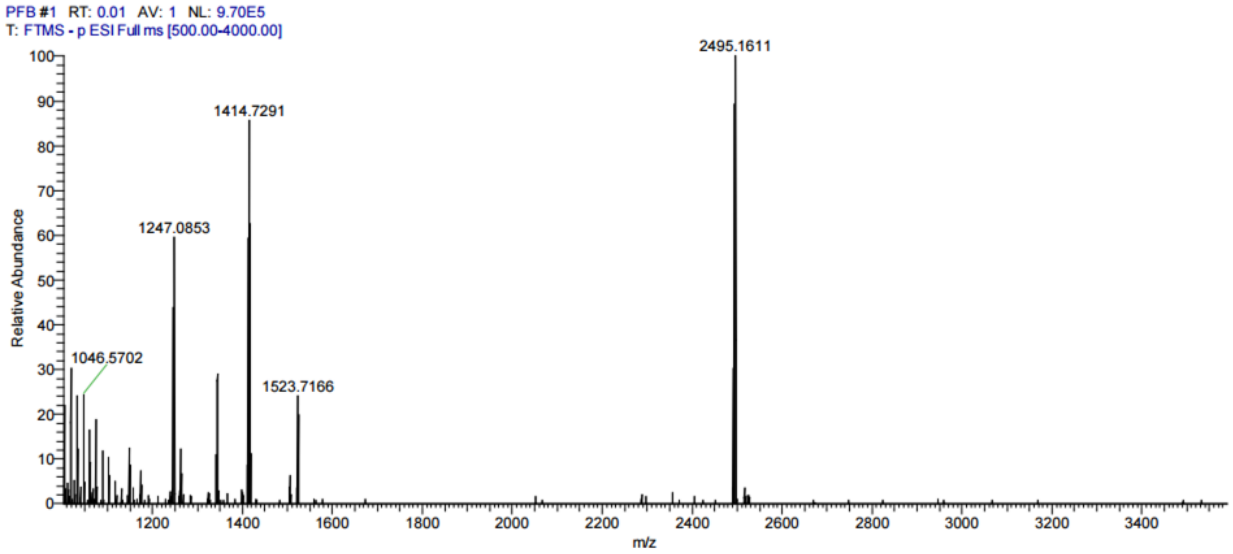

Figure S10: HRMS spectrum of $B_{12}(OCH_2C_6F_5)_{12}$ (**1b**).

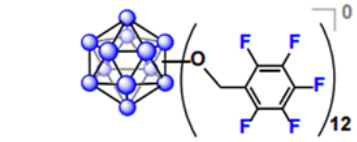

Q Exactive
High-Res Mass Spec

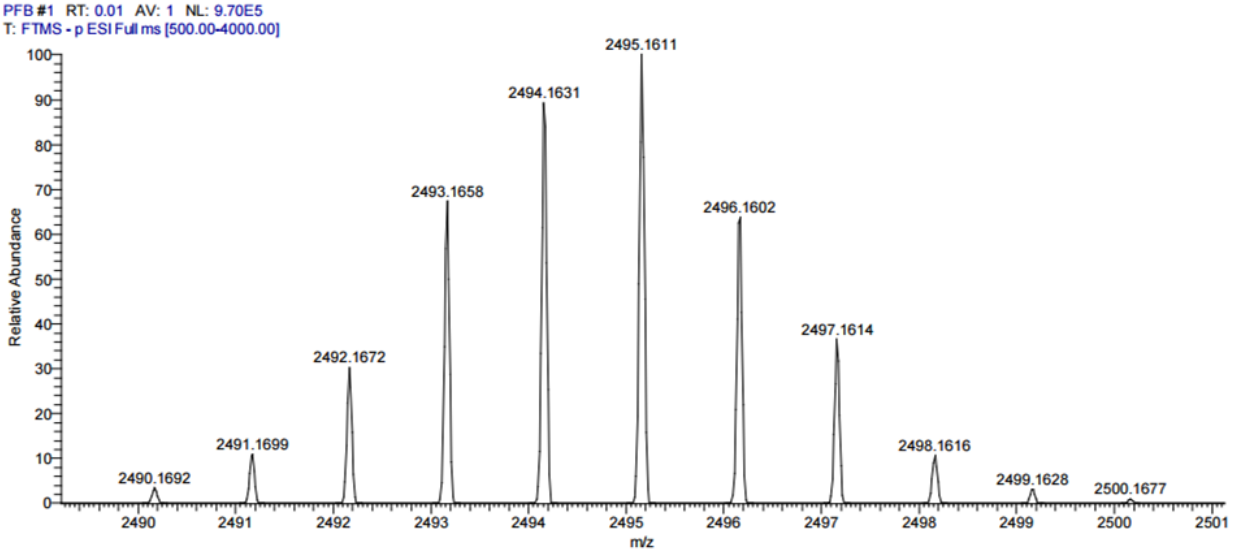

Figure S11: HRMS spectrum of $B_{12}(OCH_2C_6F_5)_{12}$ (**1b**).

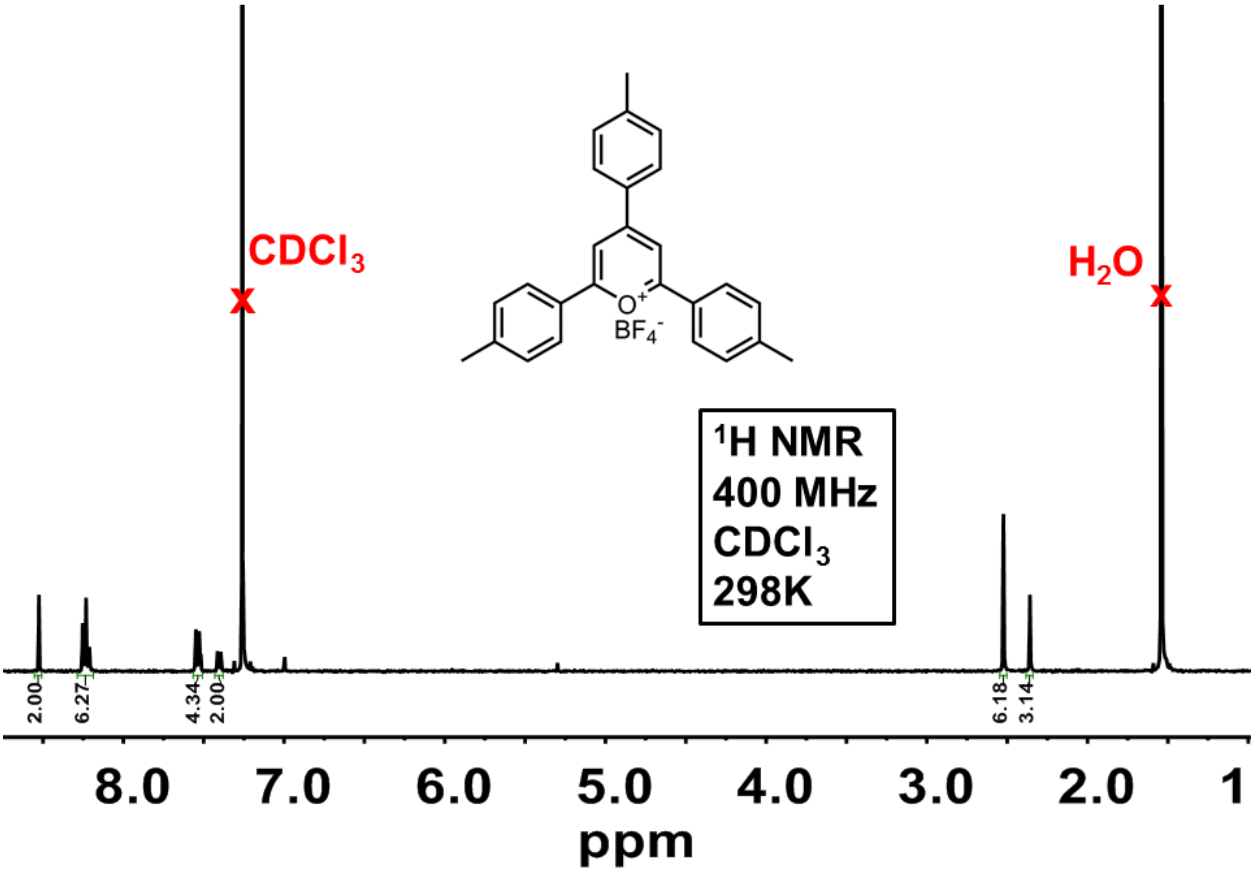

Figure S12: ^{1}H NMR spectrum of 2,4,6-tri(*p*-tolyl)pyrylium tetrafluoroborate in $CDCl_3$ at 298 K.

IV. Polymer Characterization

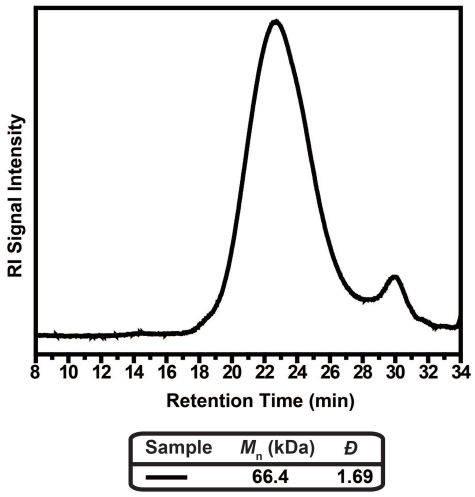

Figure S13. GPC trace from polymerization of **2a** treated with 0.5 mol% **1a** for two days. Calculated yield after precipitation is 71%. Smaller peak has a reported M_n value of 31.1 kDa and a dispersity of 1.1. GPC performed in chloroform.

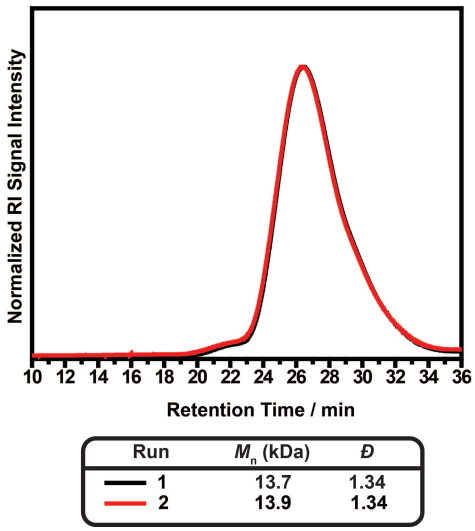

Figure S14. GPC trace overlay of a 2M solution of **2a** in CH_2Cl_2 treated with 0.5 mol% of **1a**. GPC performed in THF.

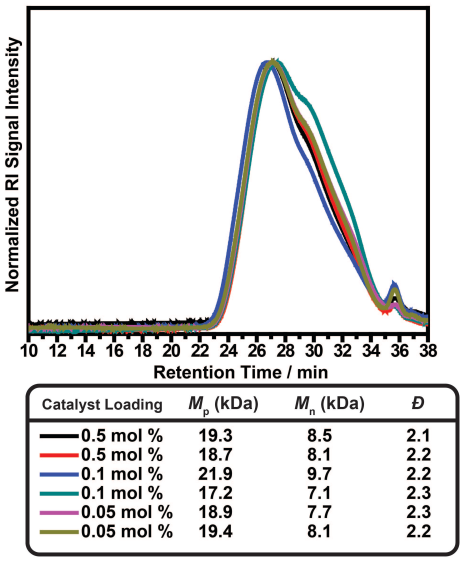

Catalyst Loading	M_p (kDa)	M_n (kDa)	$Đ$
0.5 mol %	19.3	8.5	2.1
0.5 mol %	18.7	8.1	2.2
0.1 mol %	21.9	9.7	2.2
0.1 mol %	17.2	7.1	2.3
0.05 mol %	18.9	7.7	2.3
0.05 mol %	19.4	8.1	2.2

Figure S15. GPC trace overlay of polystyrene from experiments treating styrene (**2b**) with varying concentrations of **1b**. GPC performed in THF.

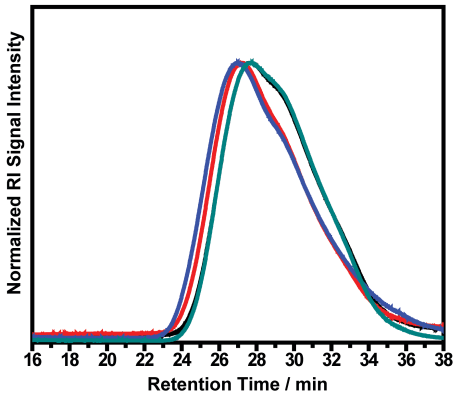

MeOH eq.	M_p (kDa)	M_n (kDa)	$Đ$
2.5	15.6	6.11	2.34
2.5	18.2	5.58	2.34
2.5	19.7	5.83	2.34
1	15.4	5.58	2.34

Figure S16. GPC trace overlay of styrene (**2b**) polymerization experiments varying concentrations of methanol to **1b** under optimized conditions. GPC performed in THF.

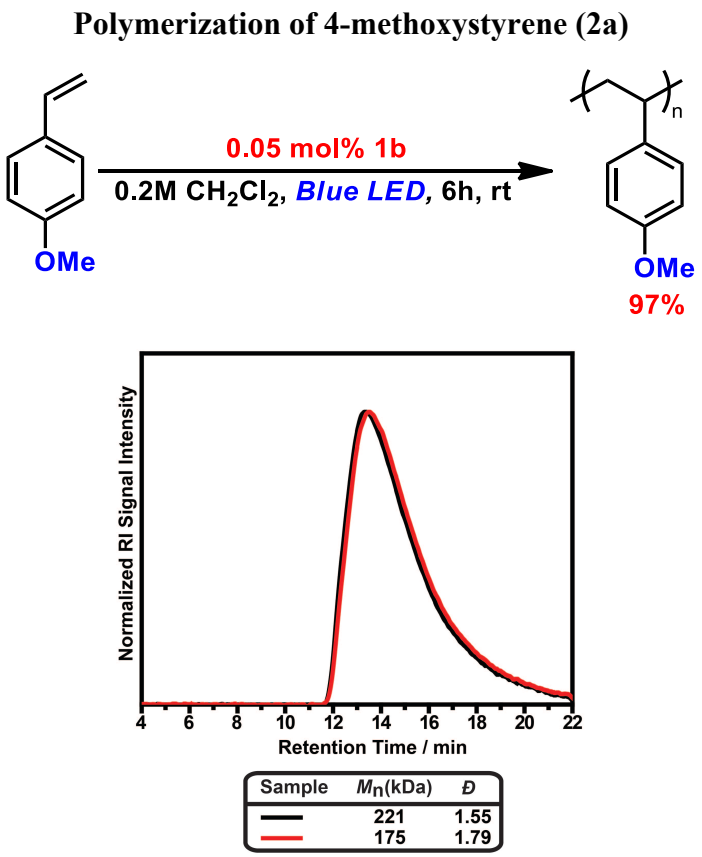

Figure S17: GPC trace overlay of poly-(4-methoxystyrene) generated using **1b** as initiator. GPC performed in DMF.

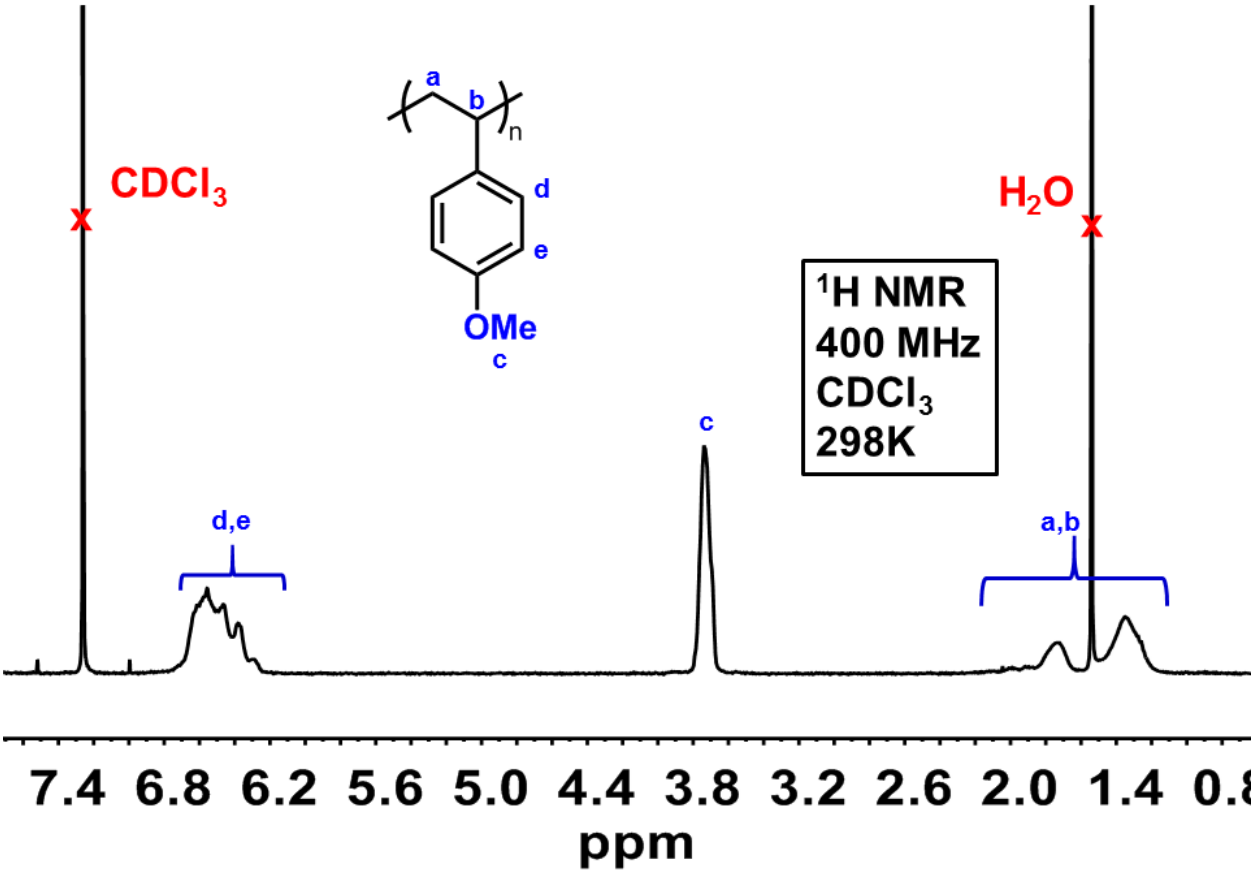

Figure S18: ^{1}H NMR spectrum of poly-(4-methoxystyrene) in $CDCl_3$ at 298 K.

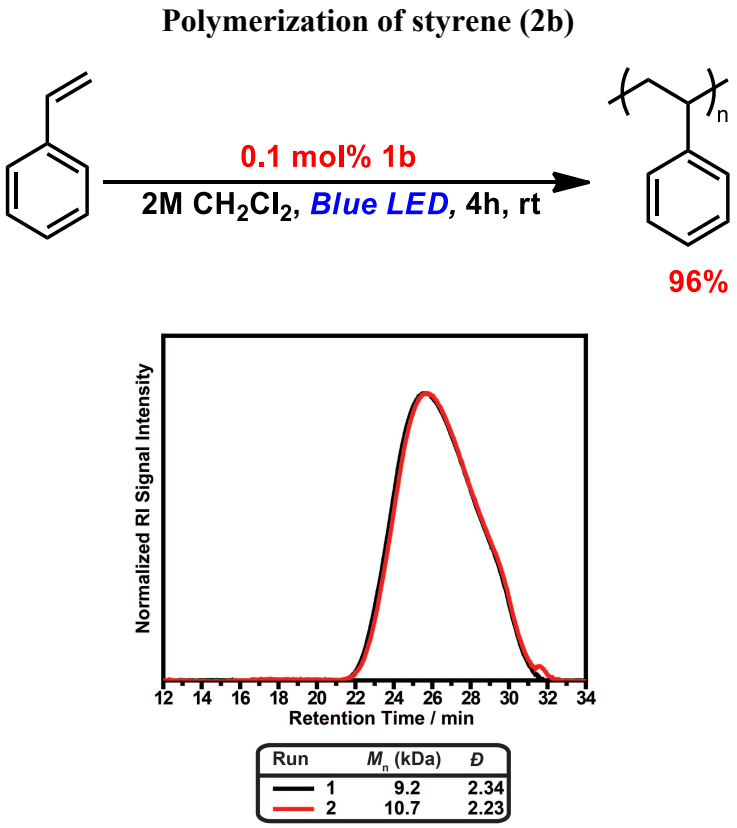

Figure S19: GPC trace overlay of polystyrene. GPC performed in $CHCl_3$.

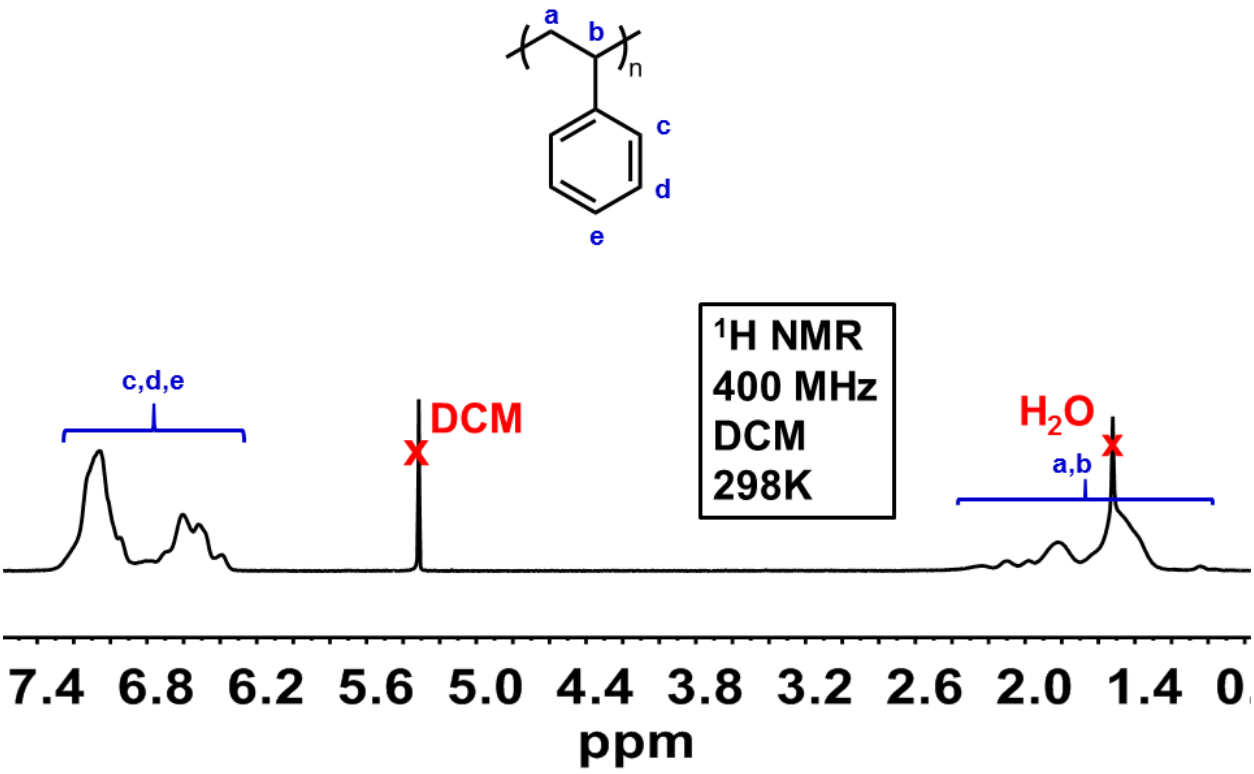

Figure S20: ^{1}H NMR spectrum of polystyrene in $CDCl_3$ at 298 K.

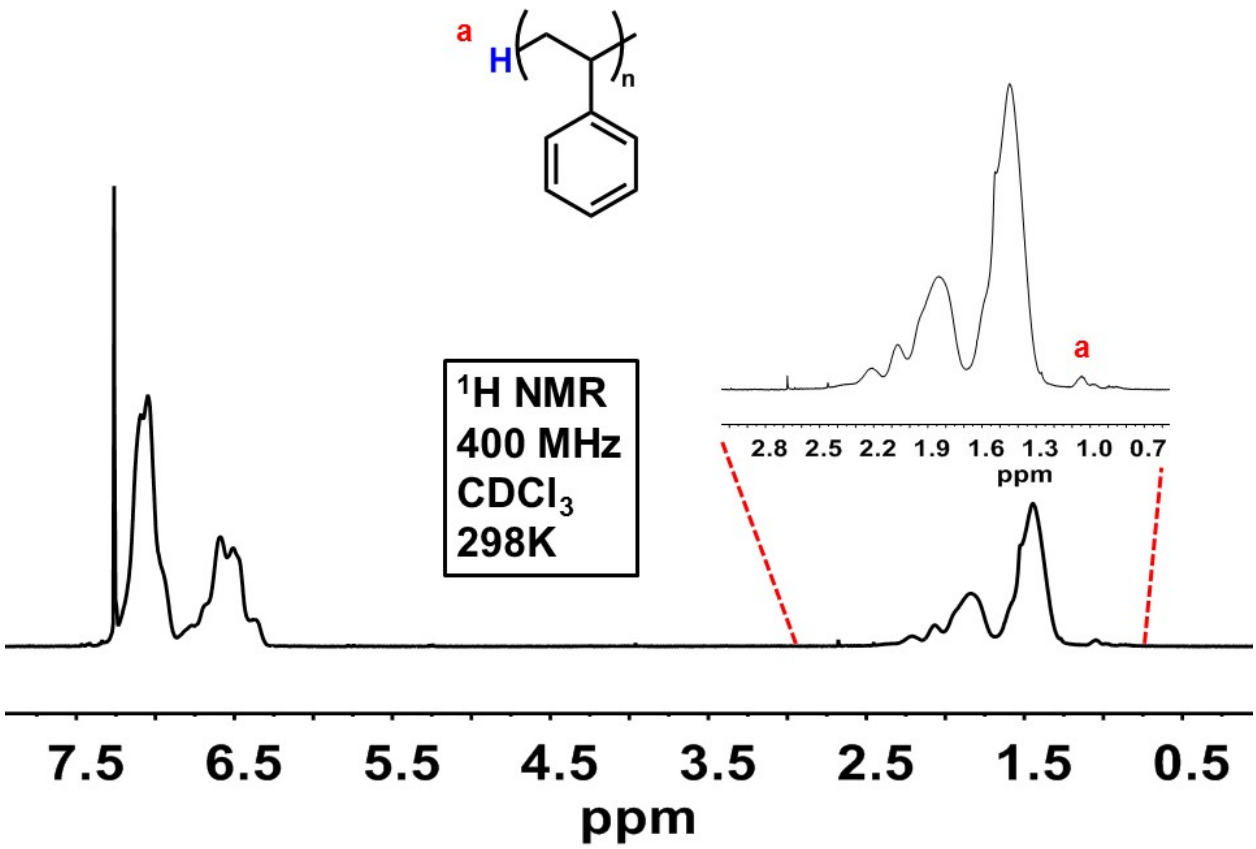

Figure S21. ^{1}H NMR spectrum of polystyrene in $CDCl_3$ at 298 K indicating the potential presence of a proton attached onto the end of the polymer.

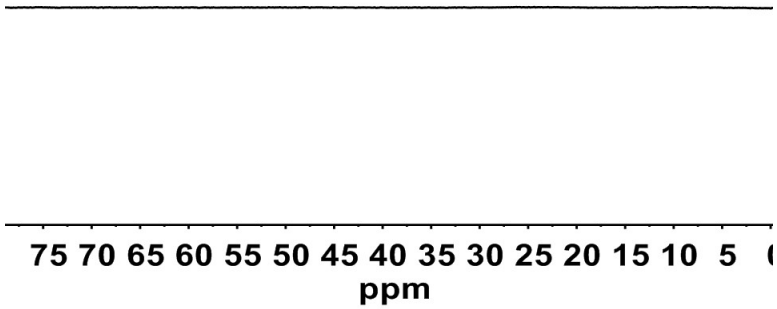

Figure S22. ^{11}B NMR spectrum of purified polystyrene synthesized utilizing optimized reaction conditions which shows that **1b** is not attaching to the polymer. Additional ICP-MS analysis on a polystyrene sample generated using **1b** determined that it contains 0.003% of boron by mass.

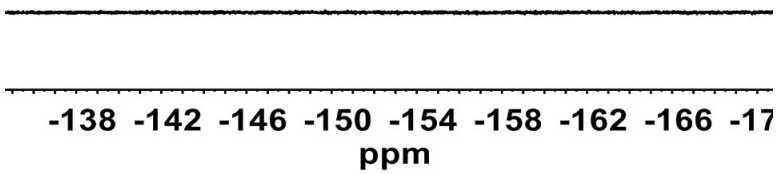

Figure S23. ^{19}F NMR spectrum of purified polystyrene synthesized utilizing optimized reaction conditions which shows that **1b** is not attaching to the polymer.

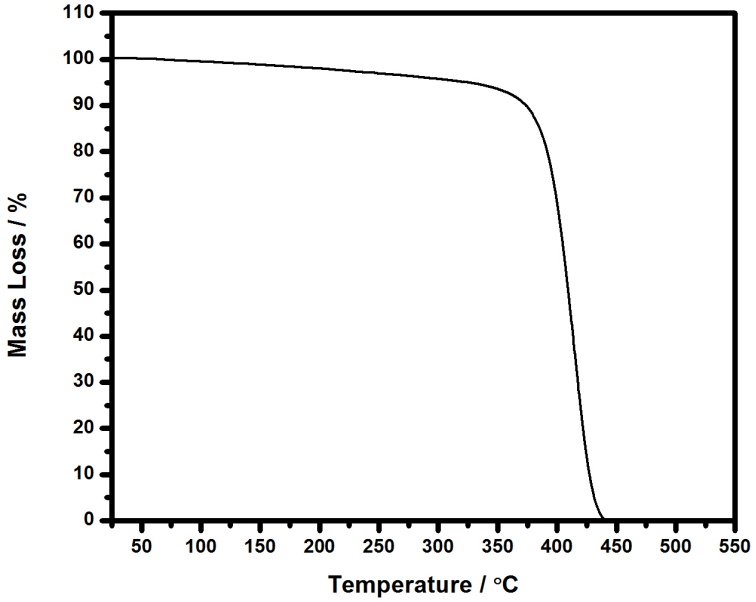

Figure S24. TGA analysis of 3.3 mg sample of polystyrene. Temperature ramping from 25 °C to 500 °C at 15 °C/min.

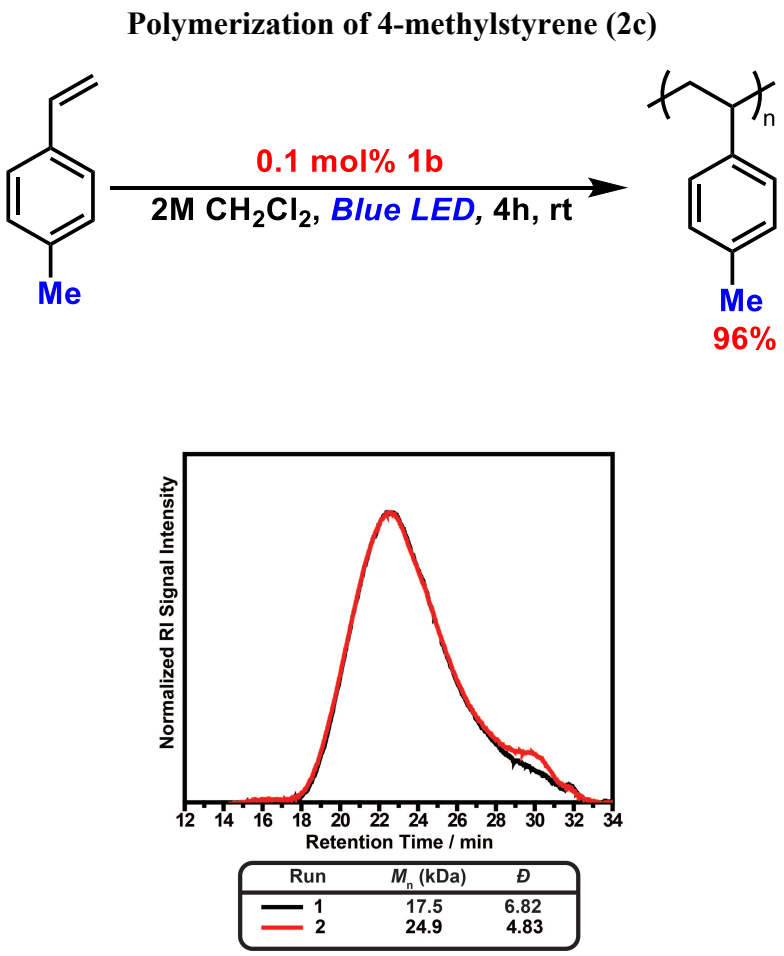

Figure S25: GPC trace overlay of poly-(4-methylstyrene).

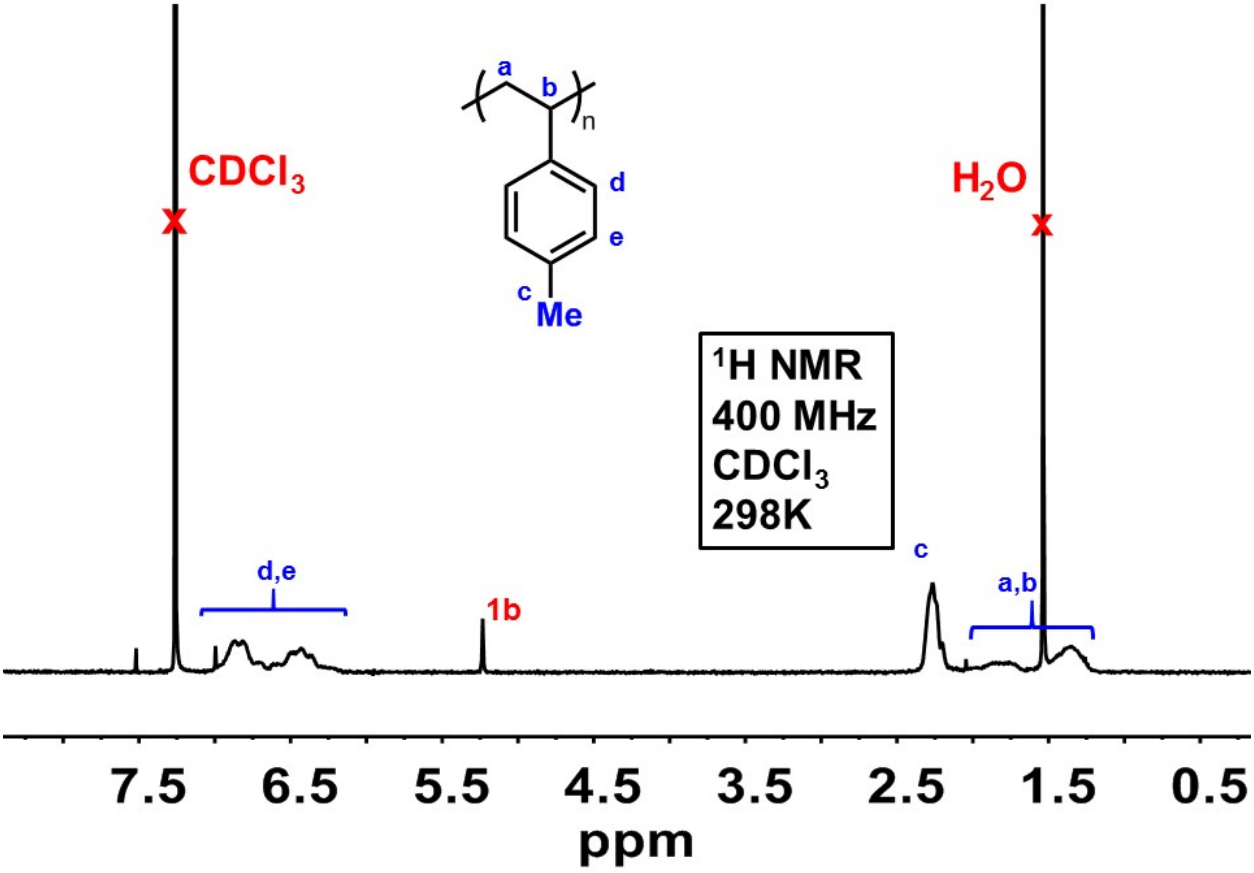

Figure S26: ^{1}H NMR spectrum of poly-(4-methylstyrene) in $CDCl_3$ at 298 K.

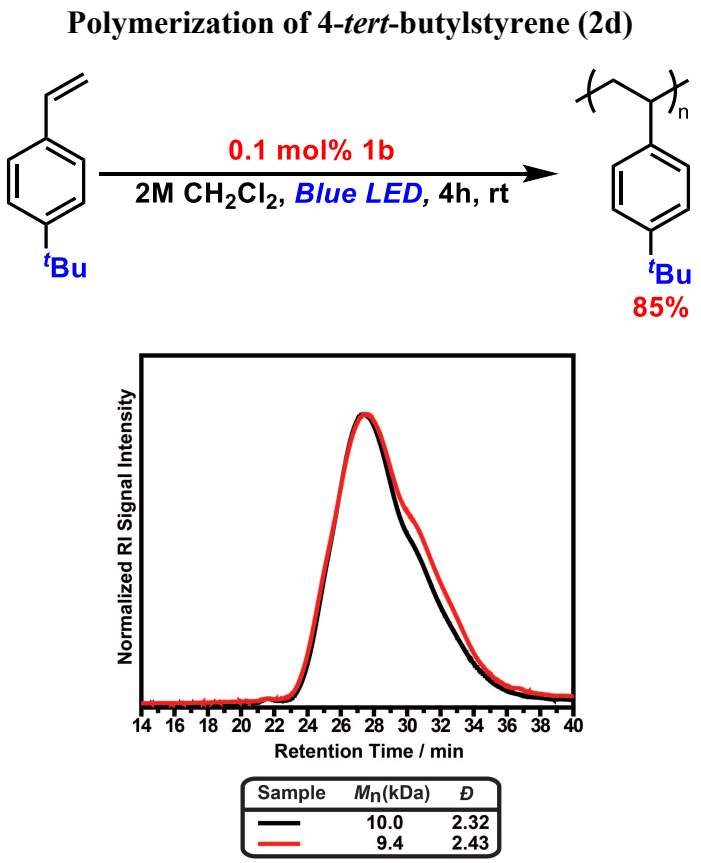

Figure S27: GPC trace of poly-(4-*tert*-butylstyrene). GPC performed in THF.

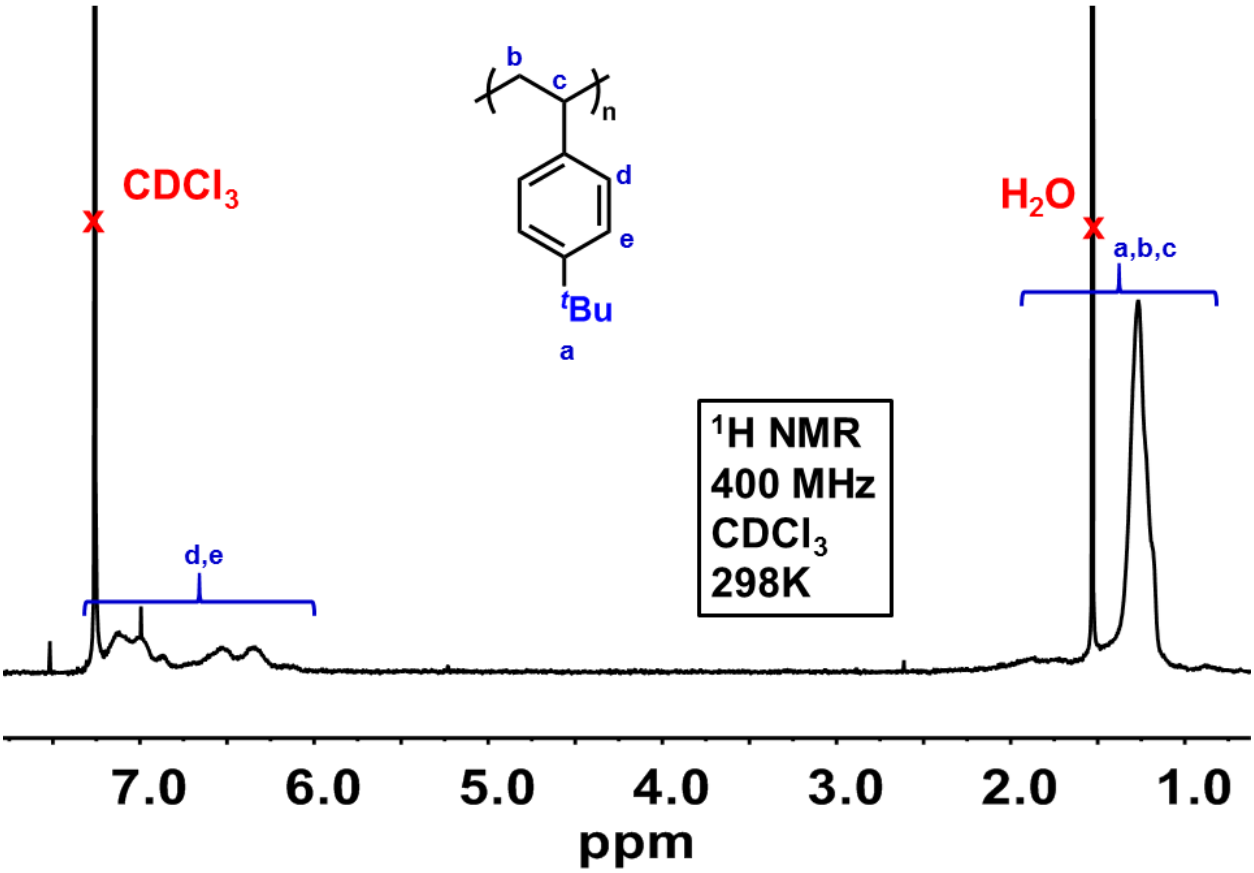

Figure S28: ^{1}H NMR spectrum of poly-(4-*tert*-butylstyrene) in $CDCl_3$ at 298 K.

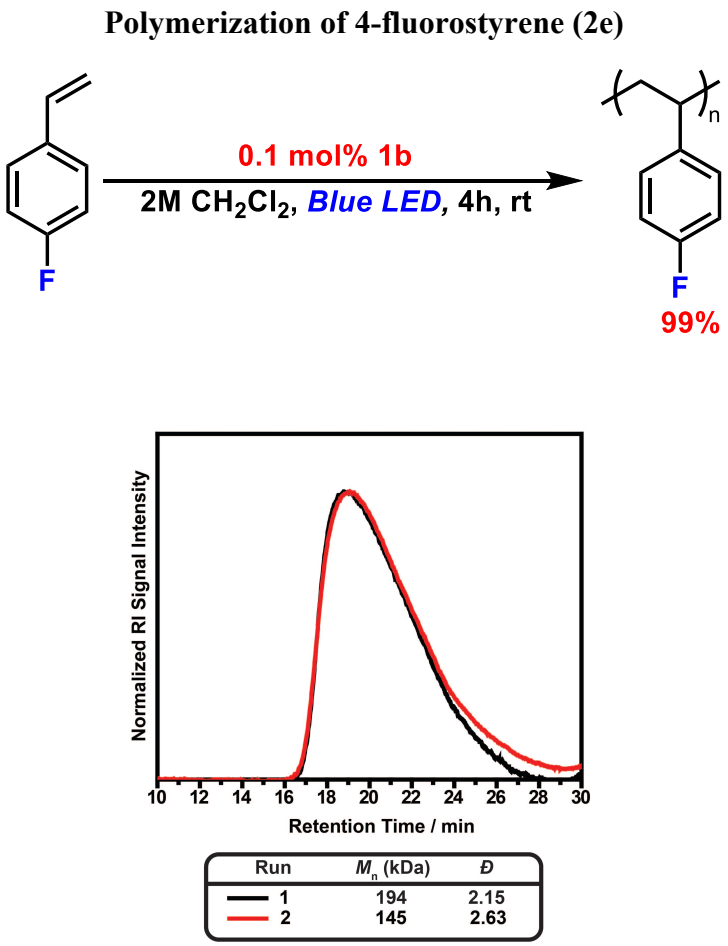

Figure S29: GPC trace overlay of poly-(4-fluorostyrene). GPC performed in $CHCl_3$.

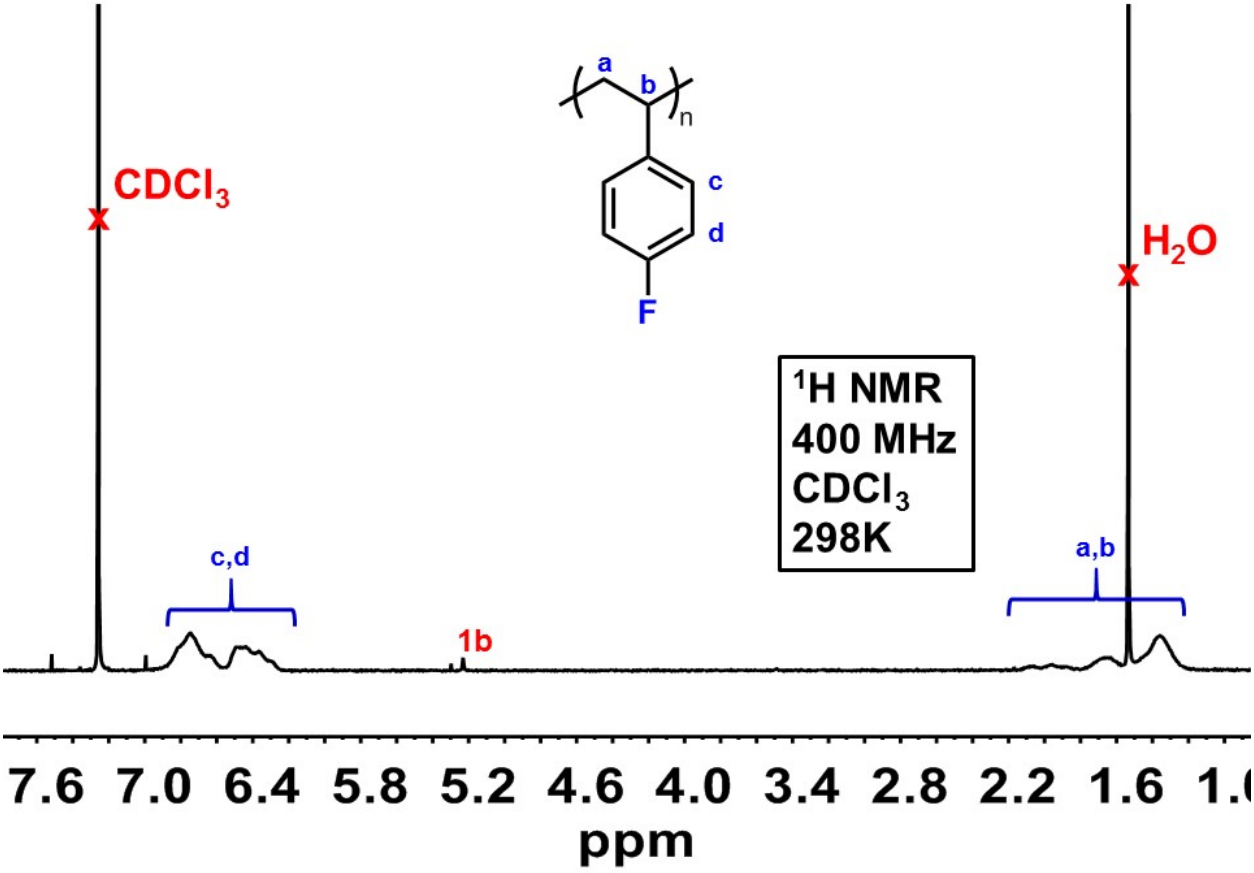

Figure S30. ^{1}H NMR spectrum of poly-(4-fluorostyrene) in $CDCl_3$ at 298 K.

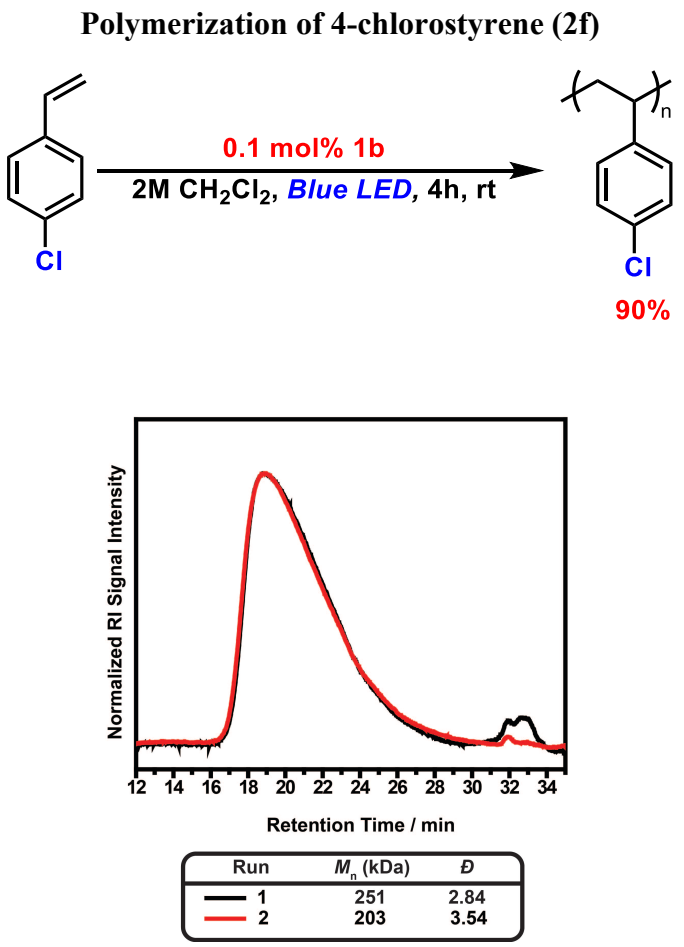

Figure S31: GPC trace overlay of poly-(4-chlorostyrene). GPC performed in $CHCl_3$.

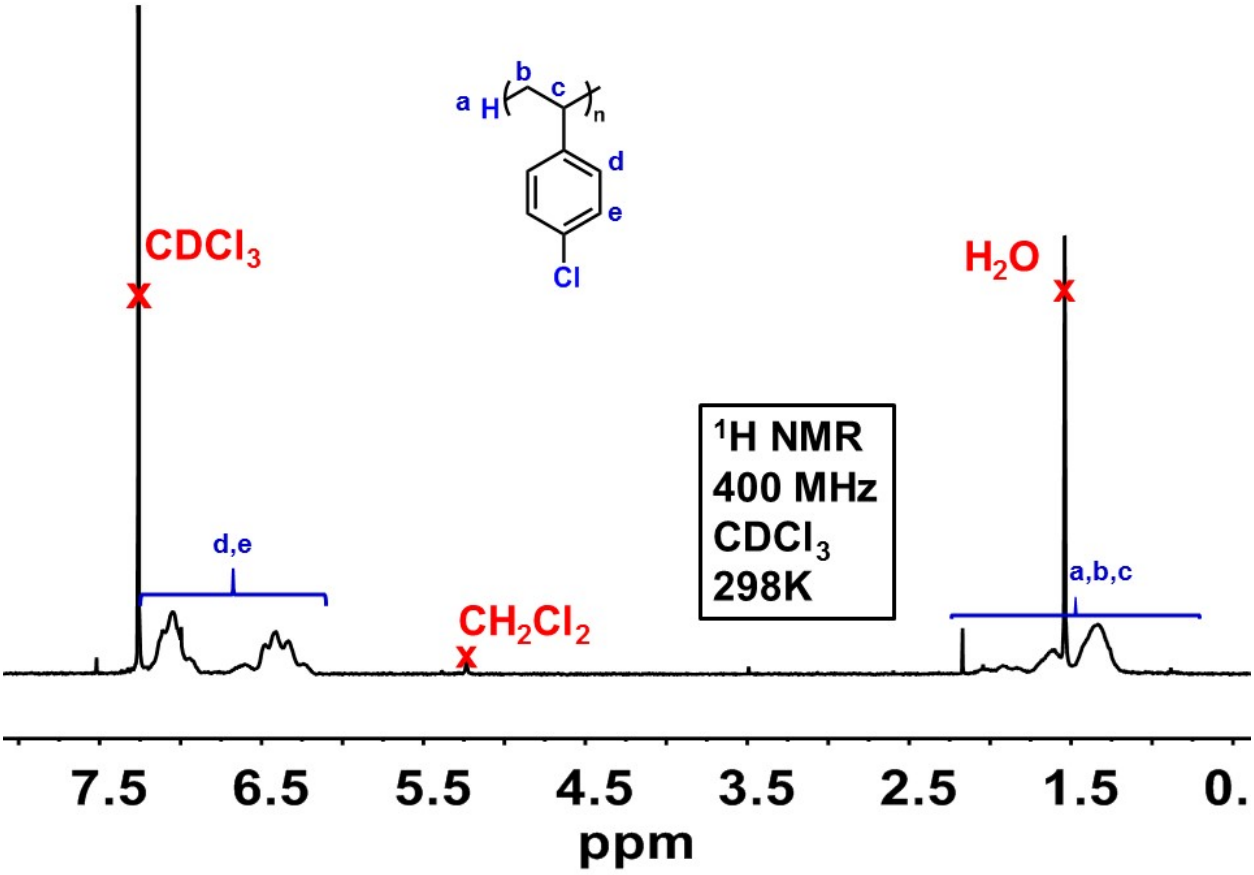

Figure S32: ^{1}H NMR spectrum of poly-(4-chlorostyrene) in $CDCl_3$ at 298 K.

Polymerization of 3-chlorostyrene (2g)

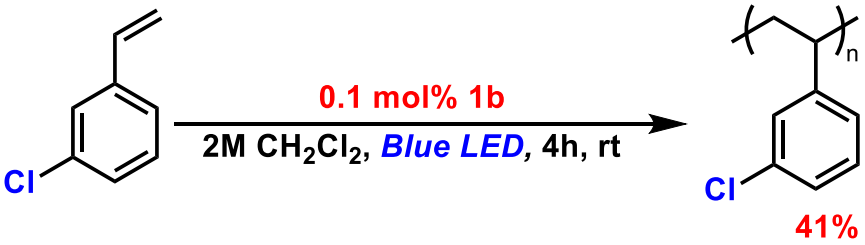

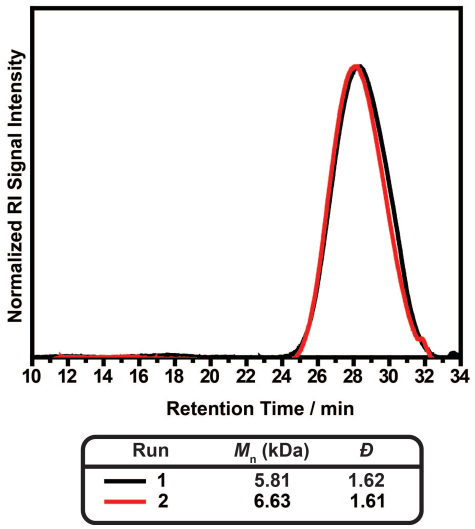

Figure S33: GPC trace overlay of poly-(3-chlorostyrene). GPC performed in $CHCl_3$.

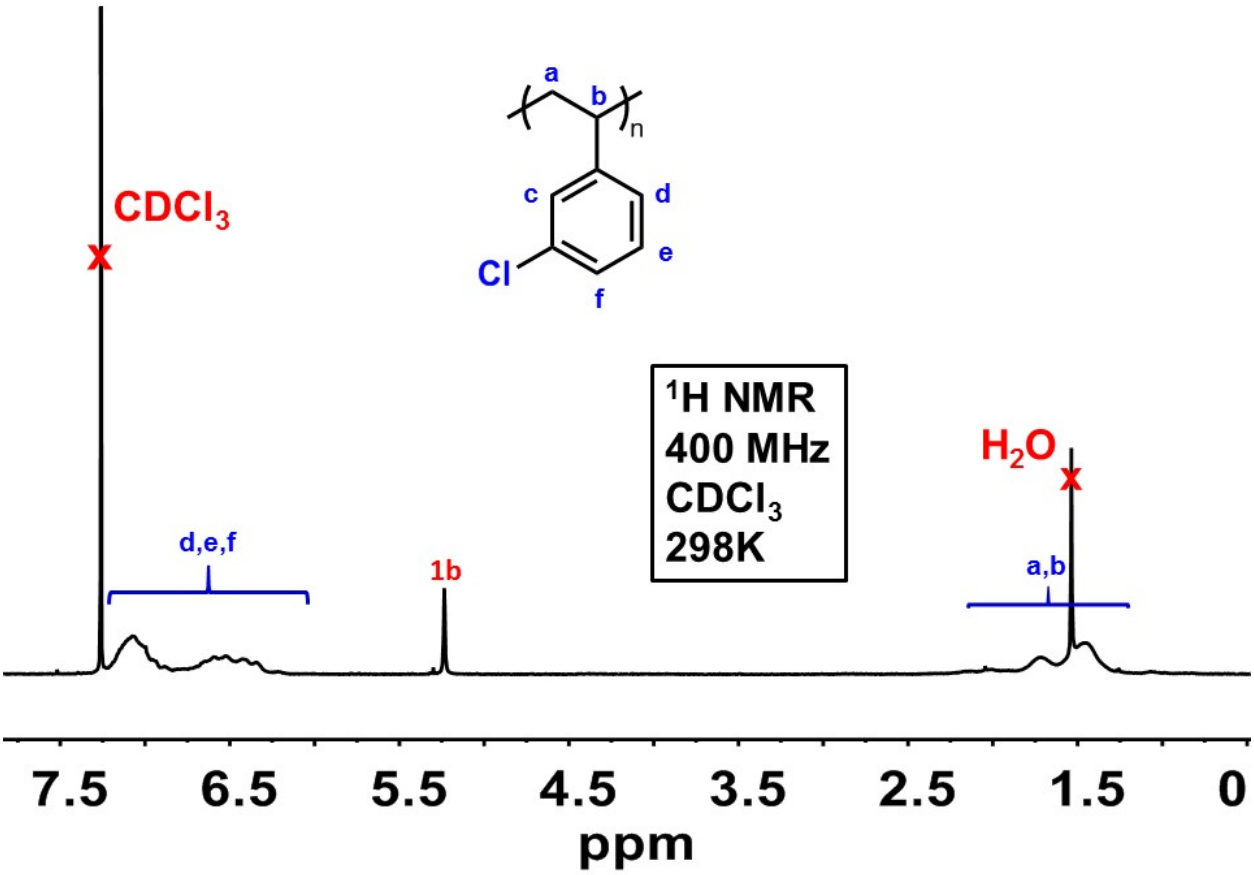

Figure S34: ^{1}H NMR spectrum of poly-(3-chlorostyrene) in $CDCl_3$ at 298 K.

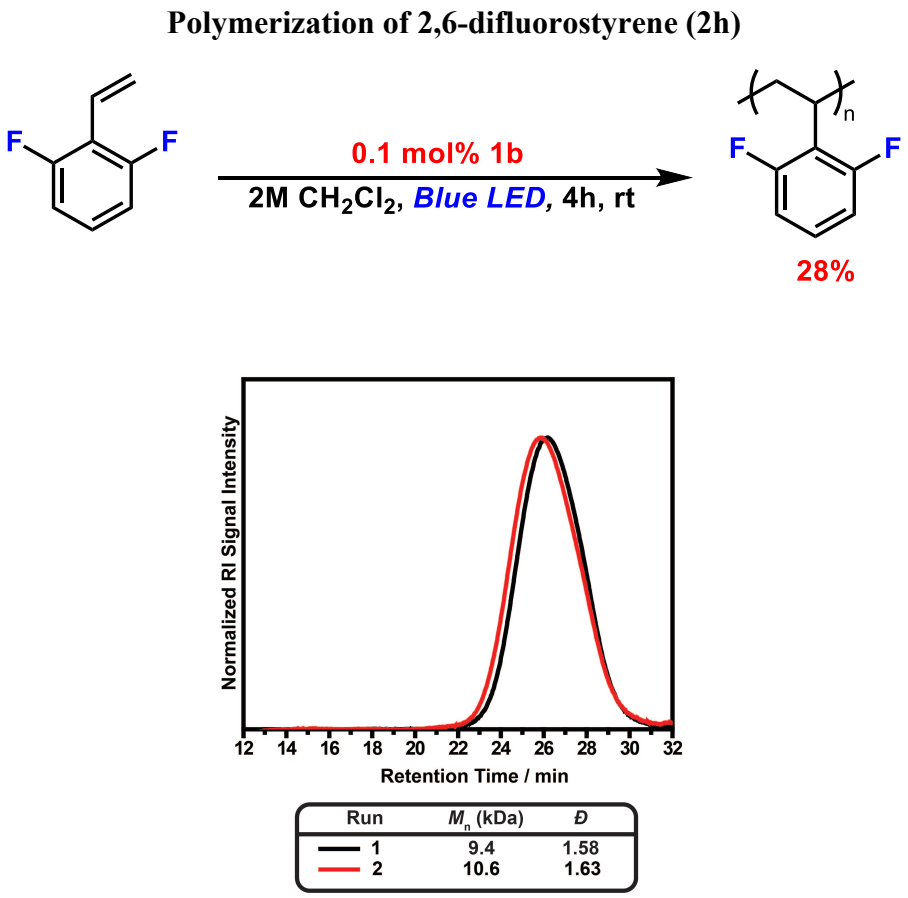

Figure S35: GPC trace overlay of poly-(2,6-difluorostyrene). GPC performed in $CHCl_3$.

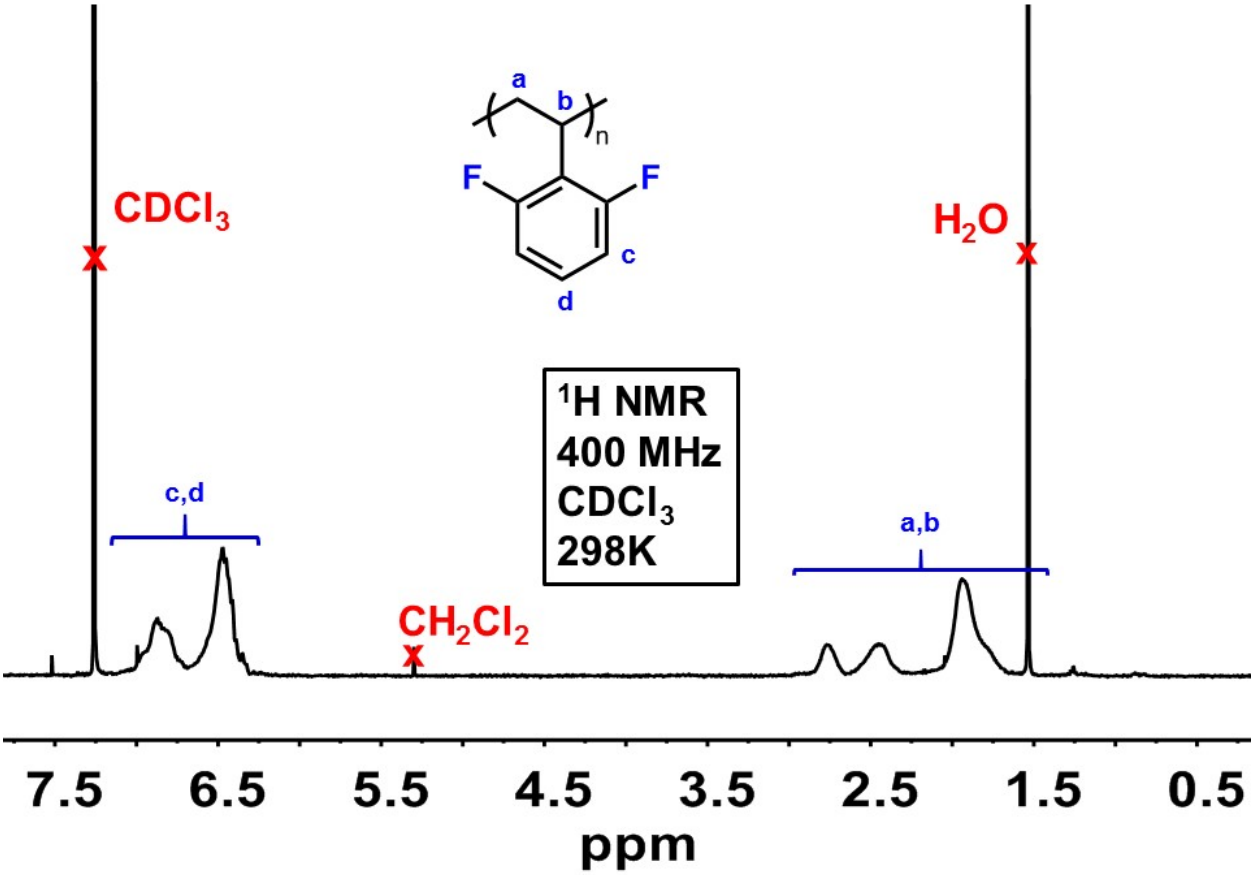

Figure S36: ^{1}H NMR spectrum of poly-(2,6-difluorostyrene) in $CDCl_3$ at 298 K.

Polymerization of 2,4,6-trimethylstyrene (2i)

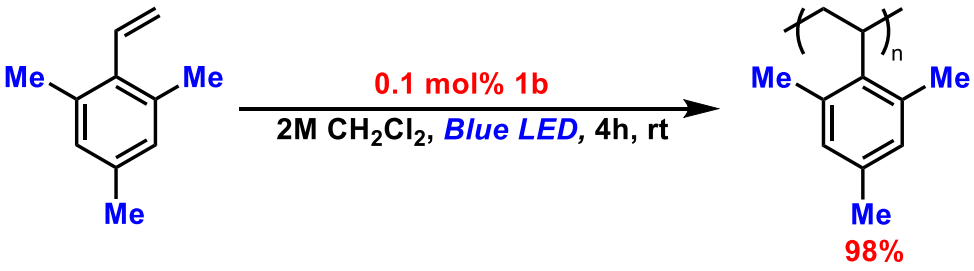

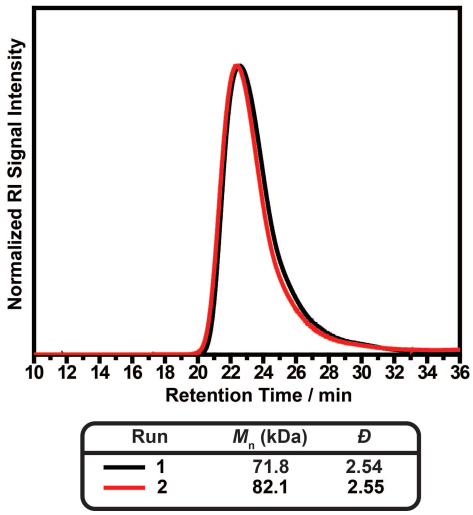

Figure S37. GPC trace overlay of poly-(2,4,6-trimethylstyrene). GPC performed in $CHCl_3$.

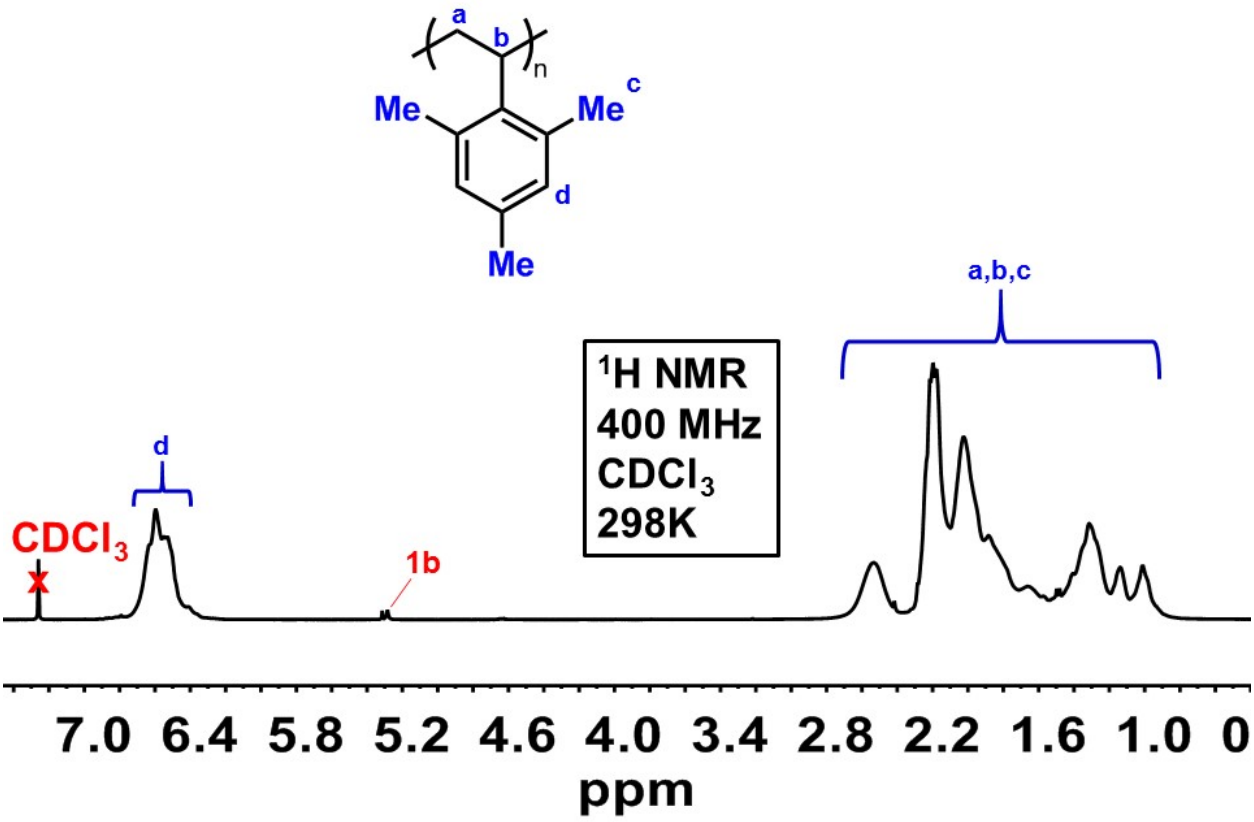

Figure S38. ^{1}H NMR spectrum of poly-(2,4,6-trimethylstyrene) in $CDCl_3$ at 298 K. Signal next to **1b** due to residual CH_2Cl_2.

Polymerization of isobutylene

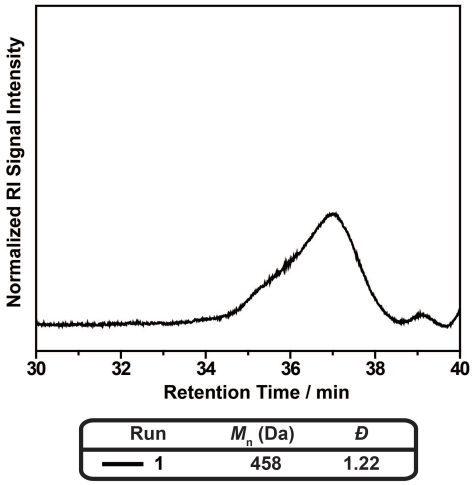

Figure S39. GPC trace of poly(isobutylene). GPC performed in THF.

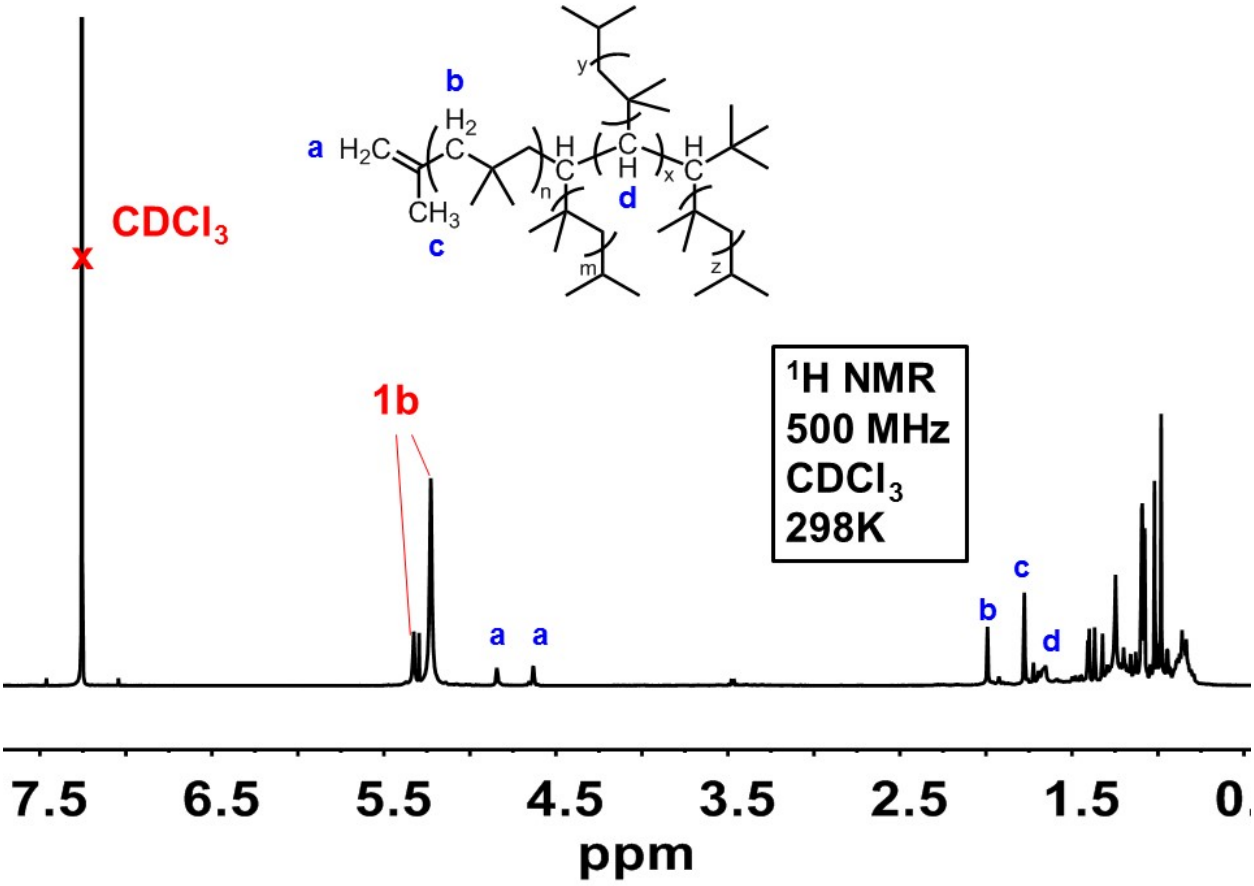

Figure S40. ^{1}H NMR spectrum of poly(isobutylene) in $CDCl_3$ at 298 K.

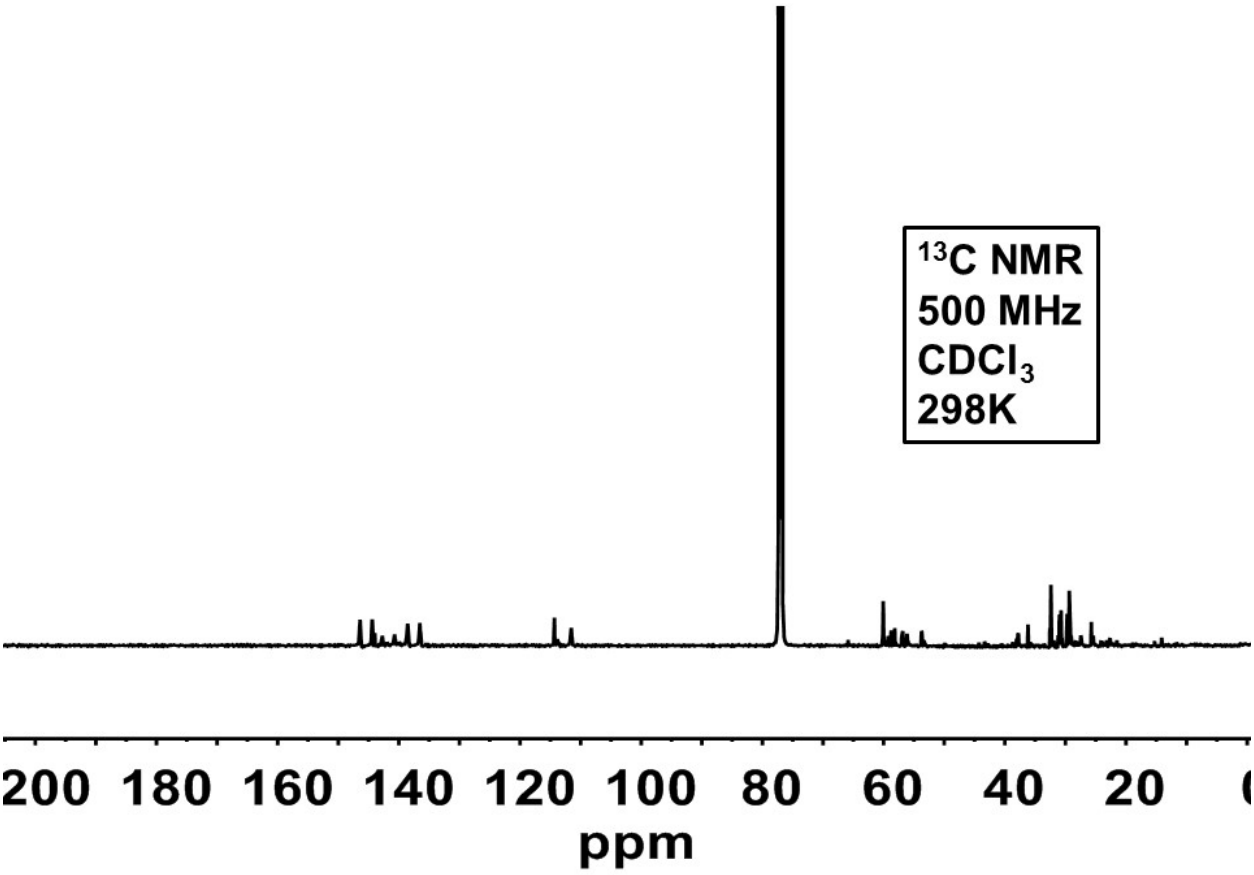

Figure S41. ^{13}C NMR of poly(isobutylene) in $CDCl_3$ at 298K.

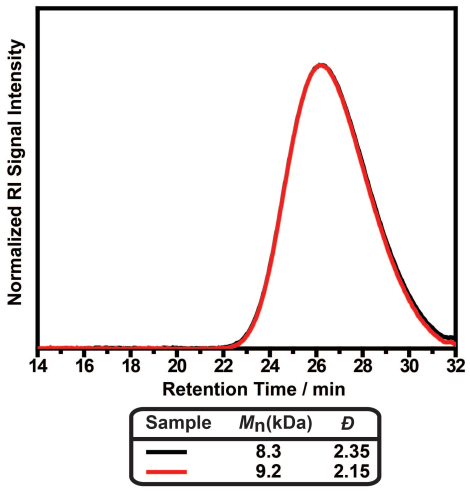

Figure S42. GPC trace overlay of optimized styrene reaction utilizing **1b** in benzene. GPC performed in $CHCl_3$.

Monomer	**Yield**	M_n **(kDa)**	**Đ**
4-methoxystyrene	97%	198	1.7
Styrene	96%	9.9	2.3
4-methylstyrene	96%	21.2	5.8
4-*tert*-butylstyrene	85%	9.7	2.4
4-fluorostyrene	99%	170	2.4
4-chlorostyrene	94%	227	3.2
3-chlorostyrene	41%	6.2	2.2
2,6-difluorostyrene	28%	10.0	1.6
2,4,6-trimethylstyrene	98%	79.6	2.6
Isobutylene	<10%	458 Da	1.2
4-fluorostyrene	21%	16.8	1.7
4-chlorostyrene	24%	9.7	1.7
4-methylstyrene	32%	31.7	2.1
Styrene	34%	5.3	1.7

Table S1. Polymer yields, M_n and $Đ$ (averaged over two runs) of polymerizations. Polymerizations of monomers in bold were prepared in ambient conditions utilizing optimized conditions (2M [monomer] in CH_2Cl_2 with 0.1 mol% **1b** and not passed through activated basic alumina.

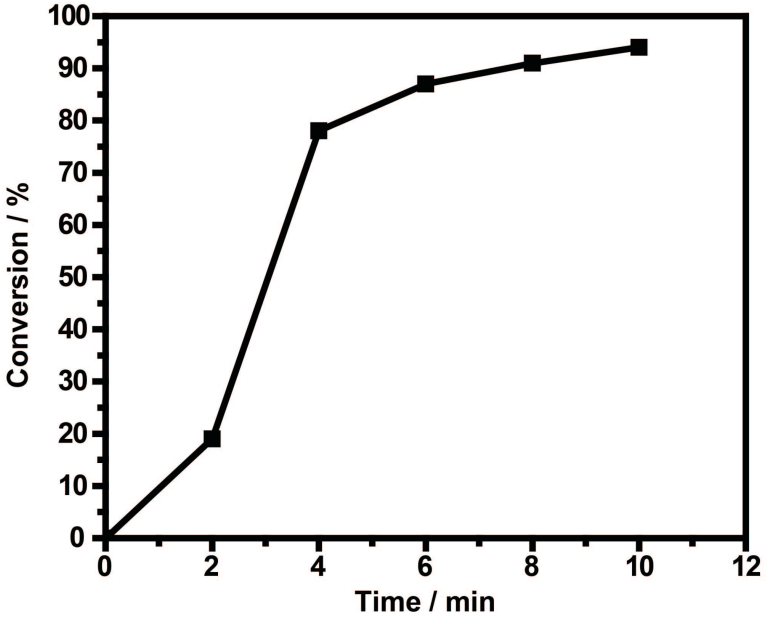

Figure S43. Conversion of optimized styrene polymerization utilizing **1b**. Time points taken every two minutes.

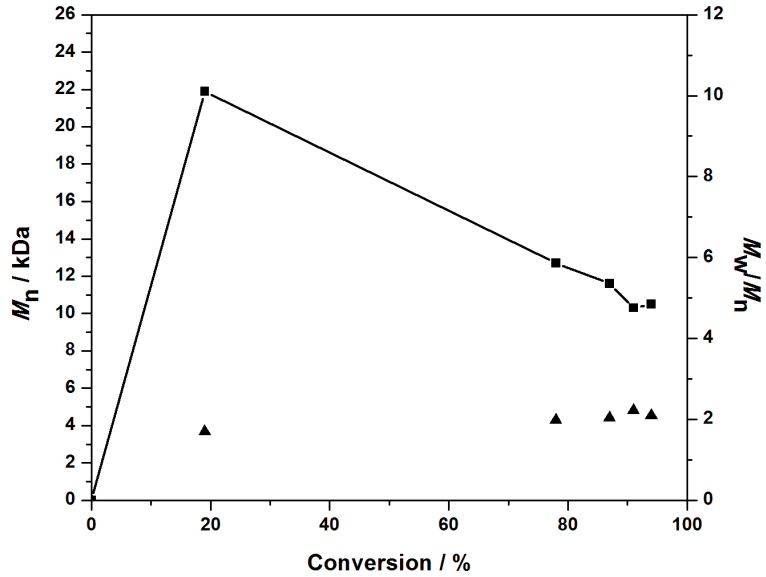

Figure S44. Conversion, M_n (Squares), and $Đ$ (Triangles) of optimized styrene polymerization utilizing **1b** (Same experiment as shown in Figure S29). The high M_n (21.9 kDa) at 20% conversion (2 minutes) followed by the drop in M_n at 80% conversion is unusual but can best be explained by the higher amount of termination events as conversion increases—there are a larger amount of shorter polymer chains as conversion increases.

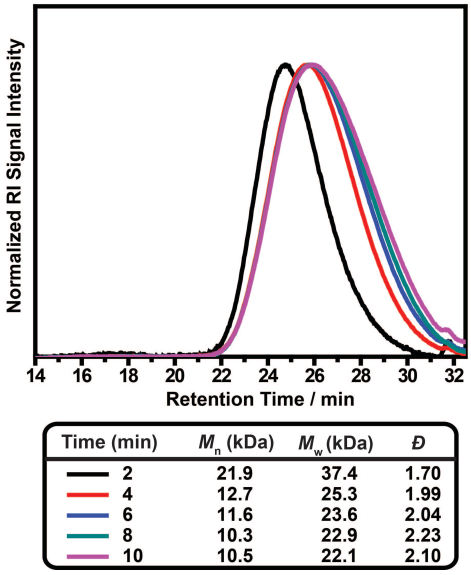

Figure S45. GPC trace overlay of optimized styrene polymerization utilizing **1b** with aliquots taken every two minutes (Same Experiment as Figure S43 and S44).

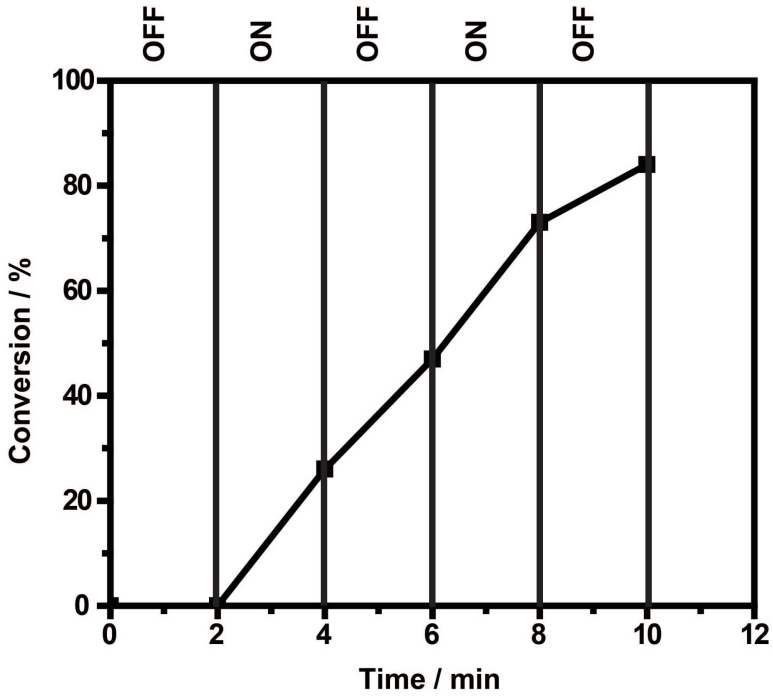

Figure S46. Polymerization of styrene under optimized conditions utilizing **1b** with light "on" and "off" cycling.

Solvent	Yield	Dispersity	M_n (kDa)	M_w (kDa)
C_6H_6	96%	2.3	8.8	19.7
$C_6H_5CF_3$	90%	3.2	5.2	16.8
1,2-$F_2C_6H_4$	92%	2.6	6.9	18.2
CH_3CN	< 5%	NA	NA	NA

Figure S47. Solvent screen (single run) for the polymerization of styrene (**2b**) in the presence of **1b** with accompanying yield, dispersity, and molecular weight data.

V. Theoretical Studies:

Methods

The geometry optimizations of the ground states of the neutral molecules were performed using *Turbomole*,[2] and the Density Functional Theory (DFT) B3LYP method,[3] with the def2-SVP[4,5] basis set. Initial coordinates were adopted from the single crystal X-ray structures of **1a** and **1b**. In order to access the energies of the unoccupied molecular orbitals (MOs) and to calculate the electronic absorption spectra, the time-dependent DFT (TD-DFT)[5,6] formalism was using with the same choice for the functional and basis set. Gaussian 09[7] was used for these calculations. GaussView[8] was used for visualization.

Computational results

Initiator structures. Figure 1 shows the optimized structures for **1a** and **1b**, and the MOs relevant to the discussion below. One may notice the oblong shapes of the optimized structures, deviating significantly from the I_h symmetry generally dictated by the B_{12} core.

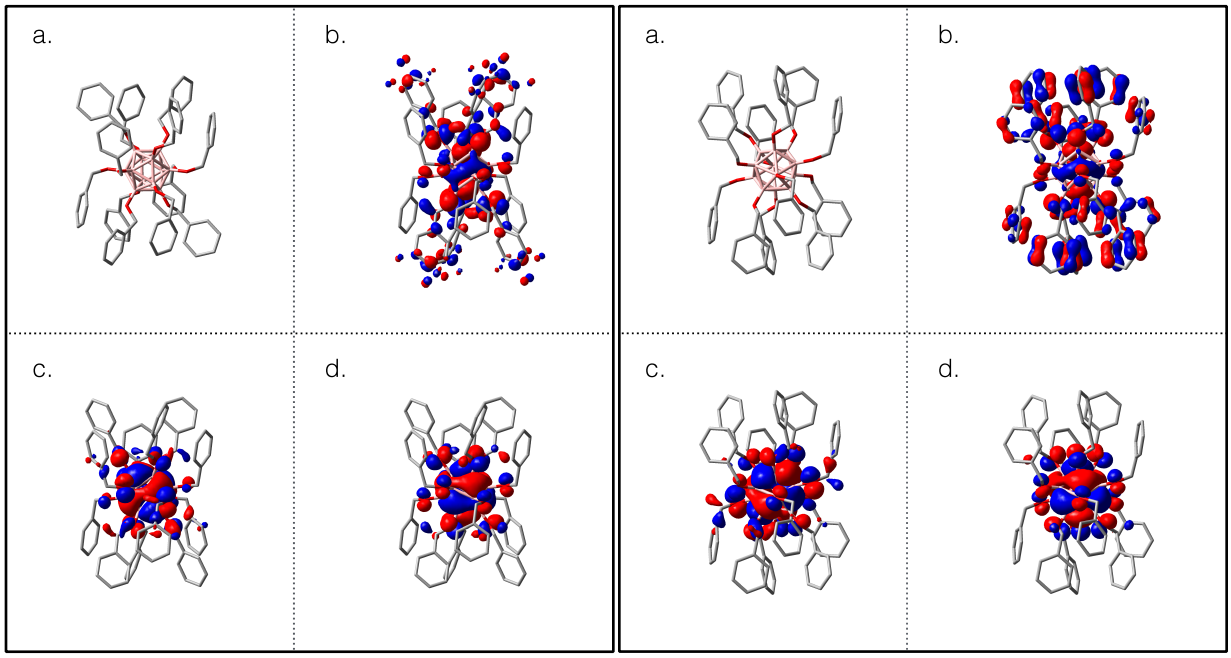

Figure S48. Optimized structures of the **1a** (left) and **1b** (right, fluorine atoms omitted for clarity) and the MOs relevant to the proposed photocatalytic mechanism. (Fig. 1, Left) a. Calculated structure, b. HOMO-15, c. HOMO, d. LUMO. (Fig1b) a. Calculated structure, b. HOMO-27, c. HOMO, d. LUMO.

Theoretical electronic spectra

The theoretical electronic spectra of **1a** and **1b** computed with TD-DFT, as described above, are shown in Tables S3 and S4, and the most relevant features are given in Tables S2.1 and S2.2 (see below). In both molecules, the HOMO to LUMO transition, and a few other transitions involving the orbitals near the HOMO were found to have near-zero oscillator strengths (i.e. being loosely

forbidden). There are very few bright transitions, which is surprising, considering the high density of states. For **1b**, the experimentally observed feature at 454 nm was assigned to the promotion of an electron from the HOMO-27 to the LUMO (both MOs are shown in Figure S40, right). The computed excitation energy was 474.07 nm (455.36 nm at M06), in a good agreement with the experiment. The HOMO-27 is the MO delocalized over the system and mainly localized on the pentafluorophenyl substituents and B-O bonds. The LUMO, on the other hand, is the MO belonging almost exclusively to the B_{12} core. Thus, the excitation corresponds to a pentafluorophenyl-to-boron cage charge transfer. For **1a**, the bright excitation involves electron transfer from the HOMO-15 to the LUMO (Figure S40, left). These MOs are very similar to those involved in the transition in **1b**. The process is again a ring-to-boron cage charge transfer. Interestingly, the calculated absorption maximum is hypsochromically shifted compared to **1b**. It is important to note that the donor orbital in **1a**, the HOMO-15, is significantly higher in energy than that of the HOMO-27 in **1b**. This is consistent with the reactivity of **1b** with a wider range of substrates than **1a**. Overall, computational characterization of the molecular and electronic structure of the photoinitiators agrees well with the experimental results, giving confidence in the performance of DFT calculations for these systems, and in theory-substantiated mechanism.

Table S2.1 TD-DFT results (at B3LYP/def2-SVP).

Initiator	Experimental Absorption (nm)	TD-DFT Absorption (nm)	Excitation Energy (eV)	Transition MOs	Energy of LUMO (eV)	Energy of Vacancy (eV)
1b	454	474.07	2.6153	HOMO-27→LUMO	-5.310	-7.925
1a	470	468.17	2.6482	HOMO-15→LUMO	-4.125	-6.773

Table S2.2 TD-DFT results (at M06/def2-SVP).

Initiator	Experimental Absorption (nm)	TD-DFT Absorption (nm)	Excitation Energy (eV)	Transition MOs	Energy of LUMO (eV)	Energy of Vacancy (eV)
1b	454	455.36	2.7228	HOMO-27→LUMO	-5.711	-8.434
1a	470	452.66	2.7390	HOMO-15→LUMO	-4.485	-7.224

Polymerization mechanism. Experimentally, the initiator is irradiated with blue LED light at 450 nm in the presence of monomer. In order to rule out the possibility of the styrene molecule undergoing the excitation at this wavelength, we calculated its absorption spectrum and found that the lowest energy bright excitation would occur at much higher energies, significantly blue-shifted from the 450 nm light source. Additionally, if styrene excitation initiated the polymerization, the reaction would proceed in the absence of **1a** or **1b**. This control experiment was performed and, as expected, no polymer was observed. Therefore, we hypothesize that the mechanism of initiation involves the electronic photo-excitation of the initiator **1a**/**1b**, resulting

in the creation of a low-lying vacancy in the valence MO manifold. The hole then accepts an electron from the HOMO of the styrene monomer, producing the stable radical anion of **1a**/**1b**; the styrene radical-cation then propagates to form polymer. This oxidation process is energetically favorable, and contributes to the driving force behind electron transfer to the initiator.

Initiator tuning. Since the proposed mechanism involves hole generation in a low-lying ring-based orbital on the initiator, followed by electron transfer from the styrene monomer to that hole, the critical component of the catalytic functional is the proper positioning of the hole with respect to the HOMO of the monomer. Thus, the MO of the initiator from which the initial excitation occurs is the one to be tuned through the nature of the ligands in order to provide a good match for the HOMO of the monomer of interest. The nature and energy of the LUMO of the initiator is less easily manipulated, since the LUMO is centered on the B_{12} core. Therefore, when the donor orbital is modulated in energy, the excitation energy will shift, possibly requiring a different light source to initiate the reaction.

Initiators **1a** and **1b**, as well as representative styrenes, were examined to further investigate this design opportunity. Four styrene derivatives were considered: 4-methoxystyrene (**2a**), styrene (**2b**), 4-methylstyrene (**2c**) and 4-fluorostyrene (**2e**). These molecules differ in the energies of the HOMO (Figure S41). All of the four styrene derivatives could be polymerized in the presence of **1b** under blue LED irradiation under the same conditions. With **1a**, under the same conditions, **2a** was polymerized, albeit in low yields. We compared the energy levels of the substrates and photoinitiators, and found a reasonable explanation: the HOMO energy of styrene and its derivatives decreases as follows: **2a** > **2c** > **2e** >**2b**, spreading over ca 0.5 eV, whereas the energy of vacancy site of **1b** and **1a** differ by ca. 1.2 eV. Therefore, the driving force for monomer oxidation should decrease in the order of **2a**, **2c**, **2e**, **2b**, and the electron affinity of the hole is higher in **1b** than in **1a**. Hence, only the monomer with the highest HOMO energy, **2a**, could transfer an electron to vacancy site in **1a**, while for **1b** all four substrates are polymerized efficiently.

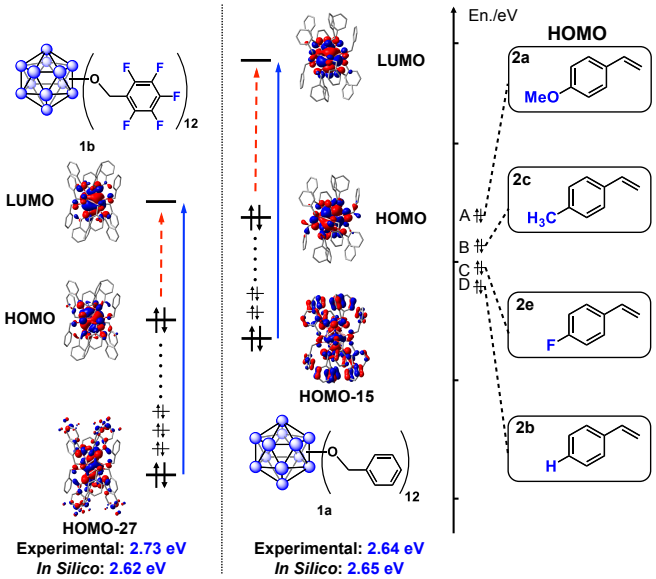

Figure S49. Depiction of the relative energy levels of initiators **1a** and **1b** with respect to the HOMO levels of monomers **2a**, **2b**, **2c**, **2e**. The schematic shows forbidden electronic transitions within the cluster core for both **1a** and **1b,** as well as the allowed (and experimentally measured) transitions (454nm and 470nm, **1b** and **1a**, respectively) from low-lying HOMO levels to a cluster-based LUMOs that give rise to monomer oxidation.

Energy calculations for relevant molecular orbitals in **1a**, **1b**, and monomers **2a**, **2b**, **2c**, and **2e** using both B3LYP/def2-SVP and M06/def2-SVP.

M06_1a

Ground State MO:
MO#357 eigenvalue = -.2654934 H = -7.224 eV

HOMO#372 eigenvalue = -.2255475 H = -6.137 eV

B3LYP_1a

Ground State MO:
MO#357 eigenvalue = -0.248912 H = -6.77324eV

HOMO#372 eigenvalue = -0.208523 H = -5.674 eV

M06_2a, 2b, 2c, 2e

Ground State MO:
2a HOMO: -0.223699 H = -6.087 eV
2b HOMO: -0.235116 H = -6.398 eV
2c HOMO: -0.241813 H = -6.580 eV

2e HOMO: -0.243277 H = -6.620 eV

B3LYP_2a, 2b, 2c, 2e

Ground State MO:

2a HOMO: -0.206900 H = -5.630 eV
2b HOMO: -0.219830 H = -5.982 eV
2c HOMO: -0.227429 H = -6.189 eV
2e HOMO: -0.227245 H = -6.184 eV

B3LYP_1b

Ground State MO:
MO#583 eigenvalue=-.3006032 H = -8.180eV
MO#584 eigenvalue=-.2993478 H = -8.146eV
MO#585 eigenvalue=-.2912243 H = -7.925eV
MO#586 eigenvalue=-.2901954 H = -7.897eV

HOMO#612 eigenvalue=-0.245620 H = -6.684 eV

M06_1b

Ground State MO:
MO#583 eigenvalue=-.3197782 H = -8.702 eV
MO#584 eigenvalue=-.3175671 H = -8.641 eV
MO#585 eigenvalue=-.3099336 H = -8.434 eV
MO#586 eigenvalue=-.3086511 H = -8.399 eV

HOMO#612 eigenvalue=-.2617867 H = -7.124 eV

Full Calculated Electronic Spectrum:

Two different computational analyses were performed to calculate additional probable transitions within initiators **1a** and **1b**. As shown above, the results using either B3LYP or M06 functionals with the def2-SVP basis set closely reproduced relevant excitations to monomer initiation.

Table S3. Probable electronic transitions within **1a** and **1b** using B3LYP/def2-SVP.

1a	**(B3LYP / def2-SVP)**		
	Excitation Energy / eV	**Absorption / nm**	**Transition Probability**
Excited State 4	2.2742	545.18	0.0138
Excited State 5	2.2754	544.9	0.0138
Excited State 10	2.4149	513.42	0.069
Excited State 16	2.5821	480.16	0.0428
Excited State 17	2.5825	480.09	0.0428
Excited State 18	2.6482	468.17	0.1275
Excited State 27	2.7279	454.5	0.0381
Excited State 28	2.7287	454.38	0.0382
Excited State 36	3.634	341.18	0.2726
Excited State 37	3.8708	320.3	0.0225
Excited State 38	3.872	320.21	0.0228

1b	**(B3LYP/ def2-SVP)**		
	Excitation Energy / eV	**Absorption / nm**	**Transition Probability**
Excited State 23	2.2506	550.89	0.0206
Excited State 26	2.4187	512.6	0.016
Excited State 28	2.5084	494.28	0.0986
Excited State 29	2.5713	482.18	0.0722
Excited State 30	2.6153	474.07	0.1576
Excited State 32	3.0214	410.36	0.0122
Excited State 34	3.361	368.89	0.0653
Excited State 35	3.3707	367.83	0.0844
Excited State 37	3.6992	335.17	0.0312
Excited State 38	3.7377	331.71	0.0485

Table S4. Probable transitions in **1a** and **1b** computed using M06/def2-SVP.

1a	(M06 / def2-SVP)		
	Excitation Energy / eV	Absorption / nm	Transition Probability
Excited State 4	2.3628	524.74	0.0131
Excited State 5	2.3649	524.26	0.013
Excited State 10	2.51	493.95	0.0851
Excited State 16	2.6625	465.67	0.0529
Excited State 17	2.6635	465.49	0.053
Excited State 18	2.739	452.66	0.1235
Excited State 26	2.8195	439.73	0.0248
Excited State 27	2.8201	439.65	0.0249
Excited State 36	3.7614	329.62	0.2485
Excited State 37	3.9588	313.19	0.0221
Excited State 38	3.9597	313.12	0.0221

1b	(M06 / def2-SVP)		
	Excitation Energy / eV	Absorption / nm	Transition Probability
Excited State 12	2.0612	601.5	0.0751
Excited State 18	2.2581	549.07	0.0456
Excited State 28	2.6378	470.03	0.0431
Excited State 29	2.6388	469.85	0.0434
Excited State 30	2.7228	455.36	0.1733
Excited State 36	3.5637	347.91	0.0158
Excited State 37	3.7697	328.9	0.0454
Excited State 38	3.7718	328.71	0.0454

VI. Fluorescence Spectroscopy:

Steady-state fluorescence profiles were obtained with 457.9 nm excitation (Coherent Innova 70 argon-ion laser). Luminescence was collected using an optical fiber optic and directed to a Melles Griot 13 FOS 200 spectrometer. A 457.9 nm long-pass cutoff filter was used to reject excitation light.

Fluorescence decay measurements were performed as previously described.[9,10] Briefly, a mode-locked Nd:YAG laser (Vanguard 2000-HM532; Spectra-Physic) generated ~10ps pulses which were then regeneratively amplified (Continuum) and frequency tripled to produce 355 nm sample excitation. Fluorescence was collected with a single lens and focused tonto the entrance slit of a spectrograph (Acton Research Corp SpectraPro 275). A 355 nm dielectric mirror was placed before the slit of the spectrograph to reject scattered excitation light. We observed fluorescence in two different wavelength regions: spectrograph center wavelengths of 420 or 600 nm were chosen to characterize the decay kinetics of the two fluorophores. Fluorescence decays were collected using a streak camera (C5680; Hamamatsu Photonics) in photon counting mode over a 50 ns window.

Based on ^{1}H, ^{13}C, and ^{19}F NMR studies, **1b** is the only observable species in solution, so it is likely that both observed emissions are associated with neutral **1b**. The first (420 nm) emission likely arises from the excitation of the perfluoroaromatic rings situated on the periphery of the cluster; the strong emission and longer lifetime (~4ns) are consistent with that of fluorinated aromatic systems.[11] The second, weaker emission at 600 nm, which exhibited solvent-dependent intensity and lifetime, may be associated with the cluster core.

The reduction potential of photo-excited **1b** was approximated[12] using in Eq. 1,

$$E^{*}_{red}{}^{0} = E_{red}{}^{0} + E_{0,0} \quad (1)$$

where $E_{red}{}^{0}$ represents the ground state 0/1- redox couple of **1b** and $E_{0,0}$ represents the wavelength of the onset of fluorescence (550 nm). Redox values are initially calculated based on the Fc/Fc^{+} reference and converted to SCE based on values reported by Connelly and Geiger,[13] where the formal potential of Fc/Fc^{+} referenced to SCE in CH_3CN with $[NBu_4][PF_6]$ as the supporting electrolyte is 0.40 V.

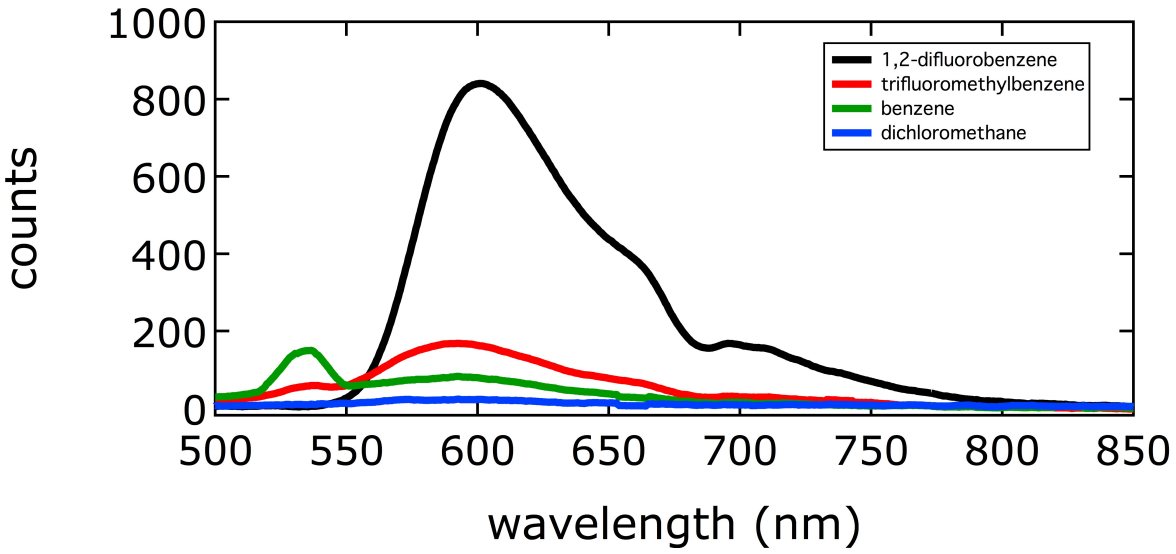

Figure S50. Fluorescence of **1b** in various solvents. Emission maximum is at 600 nm. Acquisition time was 1 s for 1,2-difluorobenzene and 2.5 s for all others.

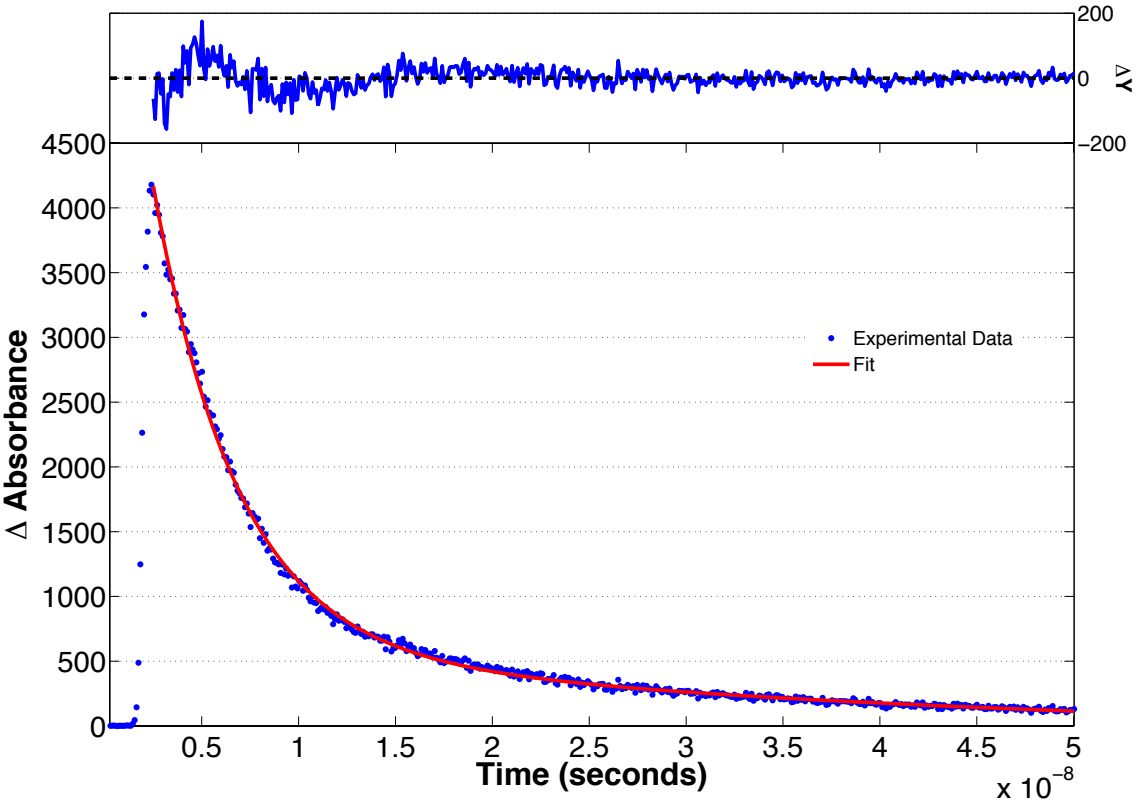

Figure S51. Fluorescence decay and fit at 420 nm for **1b** in C_6H_6. Single exponential fit gave a lifetime of 5 ns.

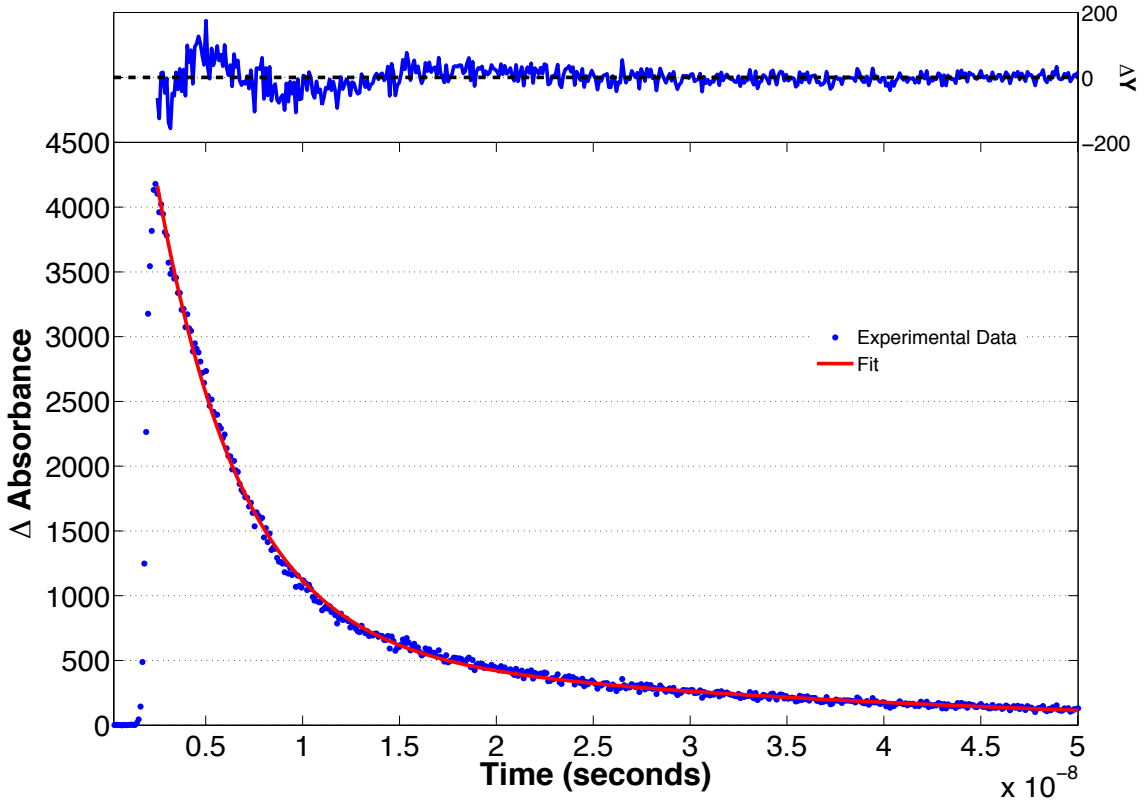

Figure S52. Fluorescence decay of **1b** in C_6H_6 at 420 nm fit to a double exponential. Lifetimes of the two species are 4 and 40 ns.

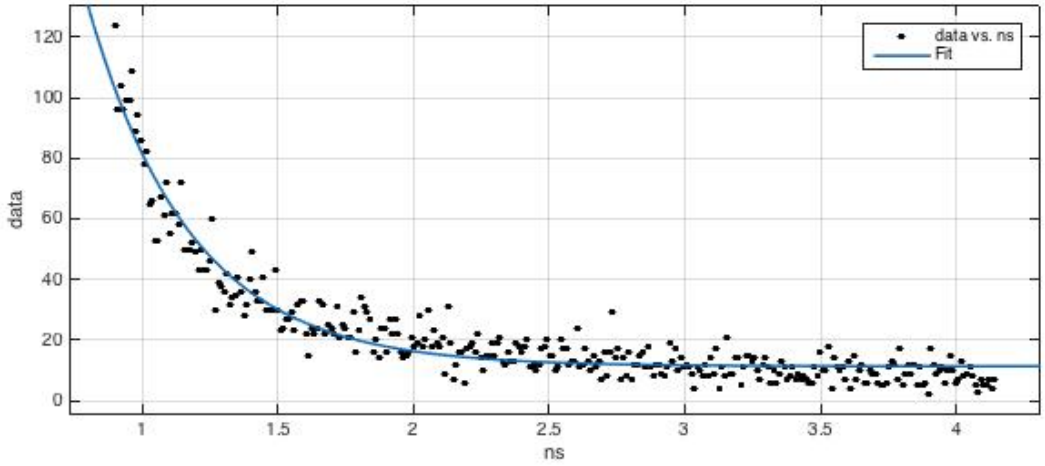

Figure S53. Fluorescence decay of **1b** in 1,2-dichlorobenzene at 600 nm. Single exponential fit gave a lifetime of 380 ps.

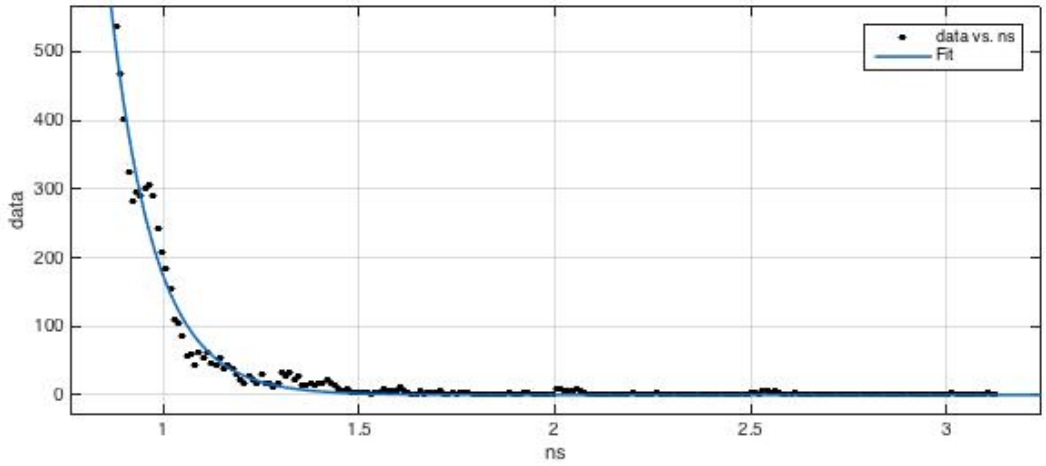

Figure S54. Fluorescence decay of **1b** in acetonitrile at 600 nm. Single exponential fit gave a lifetime of 110 ps.

VII. References

(1) a) Farha, O. K.; Julius, R. L.; Lee, M. W.; Huertas, R. E.; Knobler, C. B.; Hawthorne, M. F. *J. Am. Chem. Soc.* **2005**, *127*, 18243-18251; b) Bayer, M. J.; Hawthorne, M. F. *Inorg. Chem.* **2004**, *43*, 2018-2020.

(2) Turbomole, V6.3 2011, a development of University of Karlsruhe and Forschungszentrum Karlsruhe GmbH, 1989−2007, Turbomole GmbH, since 2007; http://www.turbomole.com.

(3) R.G. Parr, W. Yang, Density-Functional Theory of Atoms and Molecules, Oxford Univ. Press, Oxford (1989); A. D. Becke, J. Chem. Phys., 98, 1993, 5648.

(4) Weigend, F; Ahlrichs, R. *Phys. Chem. Chem. Phys.* **2005**, *7*, 3297-305.

(5) Weigend, F. *Phys. Chem. Chem. Phys.*, **2006**, *8*, 1057-65.

(6) Bauernschmitt, R.; Ahlrichs, R. *Chem. Phys. Lett.* **1996**, *256*, 454-64.

(7) Gaussian 09, Revision A.1, M. J. Frisch, G. W. Trucks, H. B. Schlegel, G. E. Scuseria, M. A. Robb, J. R. Cheeseman, G. Scalmani, V. Barone, B. Mennucci, G. A. Petersson, H. Nakatsuji, M. Caricato, X. Li, H. P. Hratchian, A. F. Izmaylov, J. Bloino, G. Zheng, J. L. Sonnenberg, M. Hada, M. Ehara, K. Toyota, R. Fukuda, J. Hasegawa, M. Ishida, T. Nakajima, Y. Honda, O. Kitao, H. Nakai, T. Vreven, J. A. Montgomery, Jr., J. E. Peralta, F. Ogliaro, M. Bearpark, J. J. Heyd, E. Brothers, K. N. Kudin, V. N. Staroverov, R. Kobayashi, J. Normand, K. Raghavachari, A. Rendell, J. C. Burant, S. S. Iyengar, J. Tomasi, M. Cossi, N. Rega, J. M. Millam, M. Klene, J. E. Knox, J. B. Cross, V. Bakken, C. Adamo, J. Jaramillo, R. Gomperts, R. E. Stratmann, O. Yazyev, A. J. Austin, R. Cammi, C. Pomelli, J. W. Ochterski, R. L. Martin, K. Morokuma, V. G. Zakrzewski, G. A. Voth, P. Salvador, J. J. Dannenberg, S. Dapprich, A. D. Daniels, O. Farkas, J. B. Foresman, J. V. Ortiz, J. Cioslowski, and D. J. Fox, Gaussian, Inc., Wallingford CT, 2009.

(8) GaussView, Version 5, Roy Dennington, Todd Keith, and John Millam, Semichem Inc., Shawnee Mission, KS, 2009.

(9) Kimura, T.; Lee, J. C.; Gray, H. B.; Winkler, J. R. *Proc. Natl. Acad. Sci.* **2009**, *106* (19), 7834.

(10) Yamada, S.; Ford, N. D. B.; Keller, G. E.; Ford, W. C.; Gray, H. B.; Winkler, J. R. *Proc. Natl. Acad.Sci.* **2013**, *110* (5), 1606.

(11) Zhicheng, Z.; Ito, Y.; Washio, M.; Kobayashi, H.; Tagawa, S.; Tabata, Y. *Radiat. Phys. Chem.* **1986**, *28*, 65-68.

(12) Gray, H. B.; Maverick, A. W. *Science* **1981**, *214*, 1201-1205.

(13) Connelly, N. G.; Geiger, W. E. *Chem. Rev.* **1996**, *96*, 877-910.